NATIONAL UNIVERSITY OF SCIENCE AND TECHNOLOGY
POLITEHNICA BUCHAREST
Doctoral School of Electrical Engineering

DOCTORATE THESIS

Multisource Piezoelectric and Thermoelectric Energy Harvesting System for Industrial Machinery

- RESUME -

Doctoral Student
engr. Claudia-Irina BORZEA

Doctorate Advisor
Prof. dr. engr. Alexandru-Mihail MOREGA

Bucharest, 2024

CONTENTS

ABBREVIATIONS **4**
ABSTRACT **5**
1. INTRODUCTION **6**
2. TWIN-SCREW COMPRESSOR AS ENERGY HARVESTING SOURCE **6**
2.1. Rotary screw compressor vibration **7**
2.2. Vibration measurement and analysis of the acquired data **7**
2.3. Thermography scanning **8**
3. PIEZOELECTRICITY **9**
3.1. Piezoelectric effect **9**
3.2. Brief history and principle of piezoelectric energy harvesting **9**
3.3. Piezoelectric energy harvesters **9**
3.4. Constitutive relations of piezoelectric materials **10**
4. PIEZOELECTRIC HARVESTING SYSTEM PROPOSED **10**
4.1. Midé PPA-4011 piezoelectric transducer **10**
4.1.1. Piezoelectric material properties 11
4.1.2. Material properties of the physical piezoelectric harvester chosen 12
4.1.3. Mathematical model particularised for the physical piezoelectric harvester 12
4.1.4. Equivalent circuit for the quadmorph piezoelectric harvester 13
4.2. Digital twin of the piezoelectric harvester **14**
4.2.1. Eigenfrequency study (modal analysis) 14
4.2.2. Frequency Domain study 15
4.2.3. Time Dependent study 15
4.3. Experimental laboratory tests **16**
4.3.1. Laboratory setup 16
4.3.2. Frequency response with swept-sine function 16
4.3.3. Time response on the spectrum analyser 17
4.4. Boosting the electric output with an optimally shaped inertial mass **17**
4.4.1. Piezoelectric harvester with no additional tip mass 17
4.4.2. Piezoelectric cantilever with concentrated inertial mass 17
4.4.3. Piezoelectric cantilever with tip curvature constraining elements 18
4.4.4. Experimental results 18
4.5. Thermal influences on the piezoelectric harvester **18**
4.5.1. Temperature dependent piezoelectric constants 19

4.5.2. Piezoelectric constants variations with temperature 19
4.5.3. Free tip case (no inertial mass) 20
4.5.4. Constrained tip case (with inertial mass) 20
4.5.5. Simulations results 21
4.6. Shape optimization of the piezoelectric harvester towards triangular section ... 22
4.6.1. Material cutoff maintaining the same inertial mass 22
4.6.2. Material cutoff maintaining same mechanical stress 24
4.7. Optimal resistive load for maximizing piezoelectric power output 25
5. THERMOELECTRICITY 26
5.1. Thermoelectric effects 26
5.2. Brief history and principles of thermoelectric energy harvesting 26
5.3. Thermoelectric generators 26
5.4. Constitutive relations of thermoelectric materials 27
5.5. Finite element method simulations with a single n-p thermocouple 27
6. THERMOELECTRIC ENERGY HARVESTING SYSTEM PROPOSED 29
6.1. TEGpro TE-MOD-10W4V-40 thermoelectric generator 29
6.2. Digital twin of the physical thermoelectric module 29
6.2.1. Geometry and boundary conditions 29
6.3. Simulations with cold side and hot side temperature boundary conditions 30
6.3.1. Stationary study 30
6.3.2. Structural frequency domain study 30
6.4. Simulations considering heat flux, improving efficiency with a heatsink 31
6.4.1. Stationary study 32
6.4.2. Time dependent study 32
6.4.3. Structural frequency domain study 32
7. EXPERIMENTAL TESTS WITH THE ENERGY HARVESTING SYSTEMS IN AN INDUSTRIALLY RELEVANT ENVIRONMENT 33
7.1. Piezoelectric system harvesting the vibrations of a rotary screw compressor ... 34
7.2. Thermoelectric system harvesting the heat of a rotary screw compressor 35
8. CONCLUSIONS, ORIGINAL CONTRIBUTIONS AND FUTURE RESEARCH 37
SELECTIVE BIBLIOGRAPHY 39

ABBREVIATIONS

AC – Alternating Current;

BDF – Backward Differentiation Formula;

Bi_2Te_3 – Bismuth telluride;

BNC – Bayonet Neill–Concelman;

CAD – Computer-Aided Design;

CPU – Central Processing Unit;

DAQ – Data Acquisition;

DC – Direct Current;

DIN – Deutsche Institut für Normung;

DOF – Degree of Freedom;

EH – Energy Harvester;

EHS – Energy Harvesting System;

EMF – Electromotive Force;

FEA – Finite Element Analysis;

FEM – Finite Element Method;

FFT – Fast Fourier Transform;

FOM – Figure of Merit;

FP – Floating Potential;

FRF – Frequency Response Function;

GND – Ground;

GSM – Global System for Mobile Communications;

ICP – Integrated Circuit Piezoelectric;

INCDT COMOTI – Romanian Research and Development Institute for Gas Turbines COMOTI;

IR – Infrared;

LED – Light Emitting Diode;

MEMS – Micro-Electro-Mechanical System;

MUMPS – Multifrontal Massively Parallel Solver;

N/A – Not Applicable;

ND – Non-Dimensional;

NUSTPB – National University of Science and Technology Politehnica Bucharest;

PARDISO – Parallel Direct Sparse Solver;

PC – Personal Computer;

PCB – Printed Circuit Board;

PDE – Partial Differential Equations;

PEH – Piezoelectric Energy Harvester;

PLC – Programmable Logic Controller;

PZT – Lead Zirconate Titanate;

PZT-5H – Lead Zirconate Titanate (soft);

RAM – Random Access Memory;

RF – Radiofrequency;

RFID – Radiofrequency Identification;

RLC – Resistor - Inductor - Capacitor;

RMS – Root Mean Square;

SHM – Structural Health Monitoring;

SSD – Solid State Drive;

TE – Thermoelectric;

TEC – Thermoelectric Cooler;

TEG – Thermoelectric Generator;

TEM – Thermoelectric Module;

TERM – Terminal;

TIM – Thermal Interface Material;

TRL – Technology Readiness Level;

VSD – Variable Speed Drive;

Wi-Fi – Wireless Fidelity;

WPC – Wireless Powered Communication;

WSN – Wireless Sensors Network.

ABSTRACT

Energy harvesting represents a very broad field encompassing technologies [1] for converting ambient energy to electrical energy, both on large scale and small scale [2], being yet a little explored field, but attracting an increasing research interest worldwide. Single source scavenging is intermittent and has limitations due to the interruptions occurring when there is not enough ambient energy available [3]. In order to overcome this issue, multisource energy harvesting [4], [5], [6] is required, using several ambient energy sources simultaneously.

The thesis focuses on developing a small-scale multisource energy harvesting system (piezoelectric and thermoelectric). The aim is to harness the energy from the vibrations and heating effects of industrial equipment (rotary bladed machines such as compressors, gas turbine engines, etc.), in order to assess the electrical output and a future storing of enough electrical energy to power wireless sensors monitoring these machines' operation or providing structural health monitoring (SHM) or fault detection.

The thesis aims to validate on a test bench, in relevant industrial conditions, the functionality of piezoelectric harvesters and thermoelectric generators. Thus, within the present thesis, a technology readiness level between TRL 5 and TRL 6 has been achieved, by demonstrating piezoelectric and thermoelectric subsystems in relevant industrial environment.

Previous researches [7], [8], [9], [10] have shown that the output voltage from one device does not suffice to power a demo energy harvesting circuit for wireless sensor nodes (WSN). The piezoelectric alternating current outputs should be rectified with diodes bridges in order to avoid cancelling each other's electrical response if vibrating in antiphase. The rectified electric output is envisaged to charge a capacitor or a rechargeable battery, and then go through a specialized piezoelectric harvesting circuit with embedded sensors.

Thermoelectric generators, with heat sinks for achieving higher thermal to electrical energy conversion efficiency, are envisaged to harness the thermal gradient due to equipment heating during operation [11], [12].

Within the present doctorate thesis, numerical simulations and experimental tests with physical piezoelectric and thermoelectric devices have been conducted, both in laboratory as well as on a compressors test bench. It is worthwhile to mention that the two types of micro energy harvesting principles are basically regarded as incompatible. On one hand, the piezoelectric materials require vibrations and are recommended to operate near room temperature due to exhibiting a decrease in the electric response both at higher and lower temperatures, which can lead to material depolarization. On the other hand, there are the thermoelectric materials requiring high temperatures at the hot side to produce energy, but do not withstand lateral axial forces. However, on a compressor skid, it was possible to install both piezoelectric and thermoelectric devices in optimal spots, after thorough vibrational and thermal analyses.

The multisource energy harvesting system proposed, original through the author's own approach and combination of harvesters, also brings some novelty elements that have not been addressed in the existent literature, and that can be consulted in the author's submitted and published papers during the doctoral stage (2019-2024).

1. INTRODUCTION

Energy harvesting represents the procedure of capturing and converting surrounding energy into usable electric power. Energy harvesting refers to energy conversion into electricity, both on large scale, as well as on small scale. The thesis herein refers to the latter form, referred to as micro energy harvesting [13], with typical levels of harvested power ranging from nanowatts to milliwatts. Energy harvesting is one of the research directions recording an increasing interest worldwide, being encouraged for improving the effectiveness of the electrical energy consumption. Generally, a complete EH system consists of three parts (Figure 1): energy harvester, power and storage circuitry, and storage media before electric load. This thesis focuses on the first aspect, aiming to assess and boost the harnessed vibrational and thermal energy from industrial machinery.

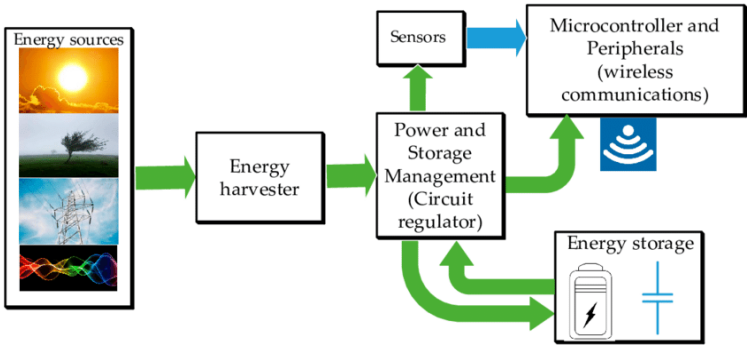

Figure 1. Energy harvesting system components [14]

The thesis focuses on developing a small-scale multisource energy harvesting system (piezoelectric and thermoelectric). The three Midé PPA-4011 piezoelectric harvesters acquired and employed in the thesis are shown in Figure 2. As well, three TE-MOD-10W4V-40 thermoelectric generators were acquired, consisting of thermoelectric pairs of bismuth telluride.

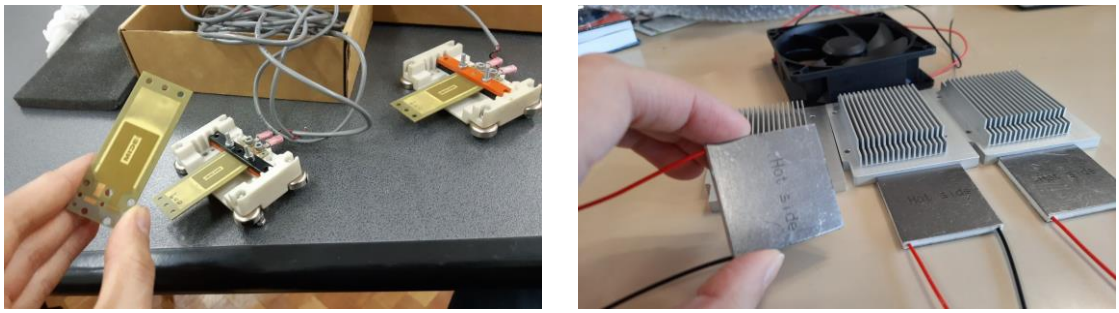

Figure 2. The three Midé PPA-4011 PEHs and TEGpro TE-MOD-10W4V-40 TEGs

2. TWIN-SCREW COMPRESSOR AS ENERGY HARVESTING SOURCE

Twin-screw compressors (Figure 3a) are rotary bladed machines used for gas compression. These ones fit within positive displacement compressors category, employing two rotors (male and female) for a progressive reduction of the volume of gas trapped between the intermeshed rotors (Figure 3b). Screw compressors give birth to strong pulsations in operation, which result in high vibration levels and noise in upstream and downstream pipes.


Figure 3. Screw compressor: design and principle (left) [15]; **b)** intermeshed rotors (right) [16]

The test bench in Figure 4 is used both for gas and air compressors.

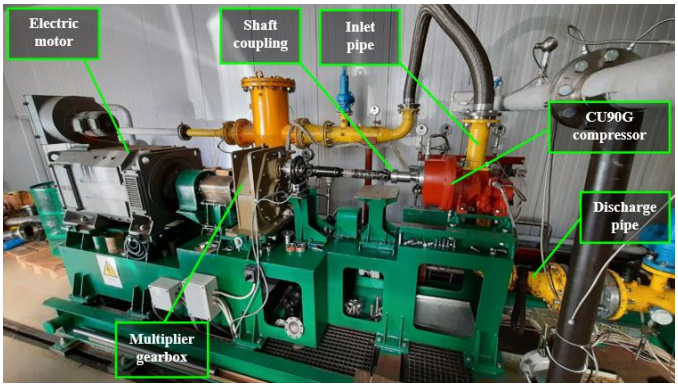

Figure 4. Compressor test bench

2.1. Rotary screw compressor vibration

The frequency can be calculated knowing the rotors' lobes number. CU90G features a driving male rotor with 5 lobes, and a driven female rotor with 6 lobes. The fundamental frequency and the frequencies of male and female rotors were calculated in Table 1.

Table 1. Calculated values of the most important compressor frequencies

No.	n_D [rpm]	n [rpm]	f_O [Hz]	f_m [Hz]	f_f [Hz]
1.	1000	2032	169.3	33.9	28.2
2.	1500	3048	254.0	50.8	42.3
3.	2000	4064	338.7	67.7	56.4
4.	2500	5080	423.3	84.7	70.6
5.	3000	6096	508.0	101.6	84.7

2.2. Vibration measurement and analysis of the acquired data

Measurements were conducted on compressor unit, using an industrial vibration analyser with a triaxial piezoelectric accelerometer. For measuring the vibrations, five points on the compressor housing known for higher vibration magnitudes (Figure 5), and four compressor speeds were considered: 1000 rpm, 1500 rpm, 2000 rpm, 2500 rpm.

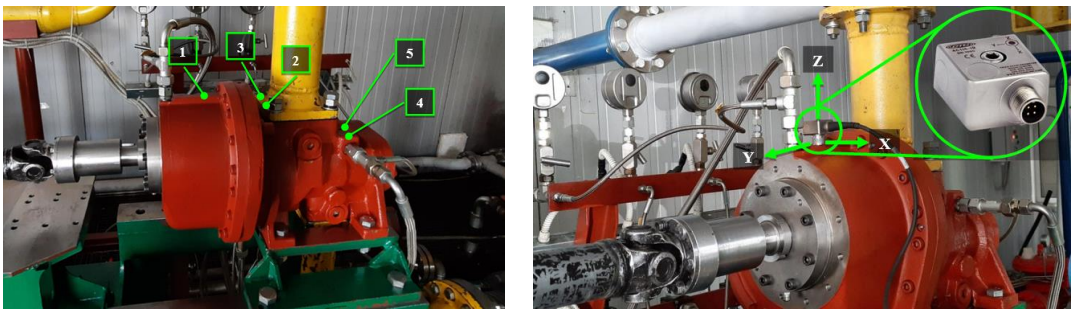

Figure 5. The five measuring points where the accelerometer was placed

Figure 6 shows the frequency spectra in point 1, at 2500 rpm running speed, with 6 bar discharge pressure. The fundamental frequency is 423.5 Hz. The male rotor frequency is 83.5 Hz and female rotor frequency is 68.5 Hz. These frequencies do not vary with pressure or measuring point, but only with speed, at 2000 rpm being 67 Hz and 55 Hz respectively.

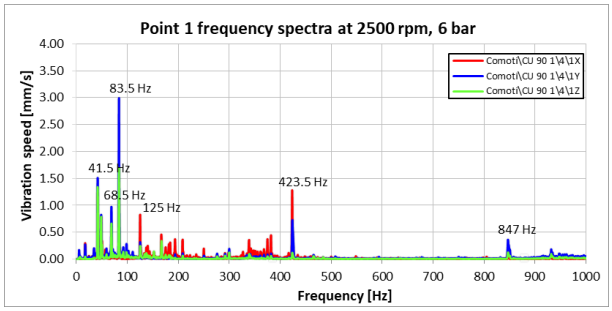

Figure 6. Vibration spectra in measuring point 1 at 2500 rpm, and discharge pressure 6 bar

2.3. Thermography scanning

The thermographic scanning is very useful for the thermoelectric generators, and also plays a crucial role for piezoelectric harvesters, vital for choosing the optimal mounting spot for PEH. As it can be observed in Figure 7, higher temperatures are exhibited in points 4 and 5, due to their closeness to the discharge port.

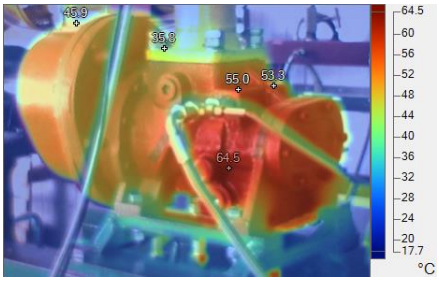

Figure 7. Thermographic image of compressor unit

Since the skid is subjected to authorization standards for its components, there are very few spots where screw mount would be possible for the TEGs installation. The chosen spot was the cover of the multiplier gearbox (Figure 8 left), splashed with hot oil from within due to shafts' rotation.

Figure 8. Screw mounting spot for thermoelectric generators and thermal scanning of gearbox cover

3. PIEZOELECTRICITY

3.1. Piezoelectric effect

Piezoelectricity is the property of certain anisotropic crystals of generating electric charge when applying mechanical stress. Piezoelectric materials are able to convert mechanical energy into electrical energy and inversely. There are two observed phenomena:

- ***Direct piezoelectric effect.*** When a piezoelectric material is subjected to mechanical stress, it generates an electric charge, proportionally to the applied stress, with a certain hysteresis. Direct piezoelectric effect is used for ***sensors*** and ***energy harvesters***.
- ***Inverse piezoelectric effect.*** When applying an electric field to a piezoelectric material, it produces strain and hence displacement, proportionally to applied electric field magnitude. Inverse piezoelectric effect is used for ***actuators***, which are more thermally insensitive.

3.2. Brief history and principle of piezoelectric energy harvesting

Piezoelectricity as research domain for the physics of crystals has started with the Curie brothers, Jacques and Pierre Curie, who discovered an unusual feature of some crystalline minerals (quartz, topaz, cane sugar, tourmaline, Rochelle salt) of generating electrical charges of opposite polarities when applying tensile and compression forces, proportionally with these forces. The phenomenon's name was assigned by Hermann Hankel, being known to this day as ***piezoelectric effect***. The term *piezoelectricity* is derived from the Greek word for pressure, *piezo*, meaning electricity from pressure [17]. A piezoelectric transducer's maximum operation temperature, which does not jeopardise the piezoelectric properties, is ***half of its Curie point***.

3.3. Piezoelectric energy harvesters

Piezoelectric harvesters employ the ***direct piezoelectric effect***, which can be used by connecting their electrodes to an electric circuit (load). When subjected to mechanical stress, piezoelectric harvesters produce electrical charge, in the form of an alternating voltage response when vibrating. A bimorph piezoelectric beam is a rectangular structure comprising two

piezoelectric layers (Figure 9). When vibrating, one of the layers compresses and the other one elongates [18]. Thus, strain is induced in the material due to the mechanical stress applied.

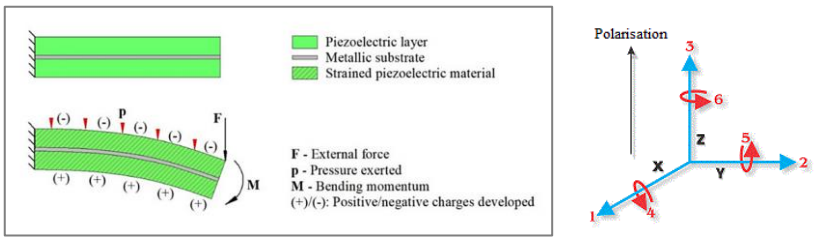

Figure 9. Piezoelectric bimorph transducer schematic (left) and polarisation axes [19] (right)

3.4. Constitutive relations of piezoelectric materials

Within piezoelectric materials, the strain and electric field are coupled through the constitutive piezoelectric relations [20], [21]. Mechanical stress and electric field can also be coupled. The ***strain-charge form***, used due to data availability, is expressed by relations (3.1):

$$\begin{cases} S = s^E T + d^T \mathbf{E} \\ \mathbf{D} = dT + \varepsilon_0 \varepsilon_r^T \mathbf{E} \end{cases} \tag{3.1}$$

where: S [ND] – strain; s^E [1/Pa] – compliance, at constant electric field; T [N/m^2] – mechanical stress; d [C/N] – piezoelectric charge constant (d^T measured at constant stress); $\mathbf{E}$ [V/m] – electric field intensity; $\mathbf{D}$ [C/m^2] – electric displacement (induction); ε^T [F/m] – electrical permittivity, at constant stress; ε_0 [F/m] – absolute permittivity of vacuum; ε_r^T [F/m] – relative permittivity, at constant stress.

4. PIEZOELECTRIC HARVESTING SYSTEM PROPOSED

4.1. Midé PPA-4011 piezoelectric transducer

The piezoelectric part of the energy harvesting system includes three Midé PPA-4011 [22] piezoceramic harvesters in cantilever construction (Figure 10). These ones were chosen adequately for the frequency ranges and power outputs of the targeted industrial machinery.

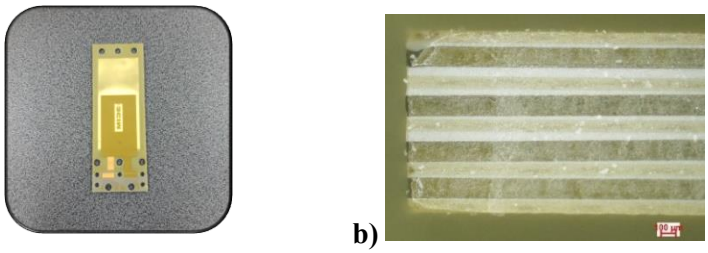

Figure 10. a) Midé PPA-4011 harvester, and **b)** side view of free tip at electronic microscope

The transducer is a quadmorph piezoelectric beam, consisting of 17 layers out of which four PZT-5H active layers. The piezoelectric harvester operates in d_{31} mode (when stress is applied on vertical axis 3, it generates charge along its horizontal axis 1). The beam's overall dimensions are 71.0 mm x 25.4 mm x 1.32 mm (Figure 11), and the total mass is 7.6 grams.

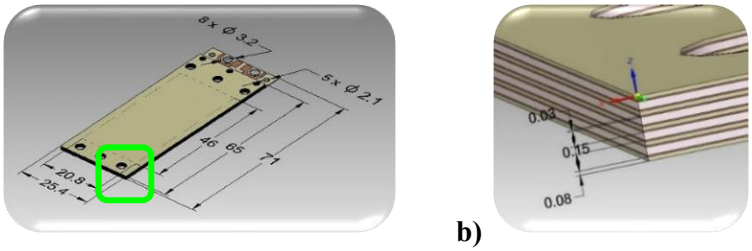

a) **b)**

Figure 11. Piezoelectric beam CAD model: **a)** isometric view, and **b)** tip corner magnification

A cantilever structure subjected to vibrations behaves like a mass-spring-damper system at the fundamental frequency. The mechanical frequency can be changed by modifying one or more variables in (4.1), for a beam of rectangular cross-section, constrained at one end.

$$f_n = \frac{1}{2\pi}\sqrt{\frac{k}{m}} = \frac{1}{2\pi}\sqrt{\frac{\frac{3YI}{L^3}}{m}} \tag{4.1}$$

where: f_n [Hz] – natural frequency; k [N/m] – stiffness constant; m [kg] – beam total mass; Y [N/m^2] – Young's modulus (equivalent); I [kg·m^2] – cross-section's moment of inertia; L [m] – beam length.

The resonant frequency can also be modified through a resonant RLC circuit, connected to the piezoelectric device. In a force-voltage analogy, the corresponding electrical quantities of a mass-spring-damper system are specified in Table 2.

Table 2. Mechanical-electrical analogue quantities in a force-voltage correspondence

Electrical	Mechanical
Inductance (L)	Mass (m)
Capacitance (C)	Compliance ($1/k$) – Inverse of spring constant (k)
Resistance (R)	Damper (c)

4.1.1. Piezoelectric material properties

For expressing the relevant terms in a convenient way, tensors of second order (for example stress and strain) are defined by 6x1 matrices comprising only unique terms. This allows expressing tensors of the third and fourth order as 6x3 and 6x6 matrices.

- *Piezoelectric charge constants*. The piezoelectric charge constants noted d_{ij} represent the polarisation generated per unit of mechanical stress, T. The given harvester operates in d_{31} mode – polarisation induced in direction 3 per unit of mechanical stress exerted in direction 1.
- *Piezoelectric voltage constants*. The piezoelectric voltage constants g_{ij} represent the electric field generated by piezoelectric materials per unit of mechanical stress applied. For direct piezoelectric effect, the first subscript i indicates the direction of electric field generated, and the second subscript j expresses mechanical stress direction.
- *Electromechanical coupling factor*. The electromechanical coupling factor k (lowercase) is an indicator of the conversion effectiveness.

- *Relative dielectric constant*. The relative dielectric constant K (uppercase) is the ratio of piezoceramic permittivity to the absolute permittivity of vacuum ε_0. The relative dielectric constant shows the amount of charge that the piezoceramic material can store, relatively to the absolute permittivity.
- *Permittivity constant*. The permittivity, or dielectric constant ε of a piezoceramic material represents the dielectric displacement per unit electric field.
- *Young's modulus*. Young's modulus, or the modulus of elasticity, Y [N/m^2] describes the piezoceramic material's stiffness, dividing applied mechanical stress to strain [23].
- *Elastic compliance*. Elastic compliance is the strain produced in a piezoelectric material per unit of mechanical stress applied.

4.1.2. Material properties of the physical piezoelectric harvester chosen

The piezoelectric properties of PZT-5H material used in Midé PPA-4011 transducer are presented within the thesis. In all the simulations conducted, the default material properties were replaced, where known, with the material properties from datasheet [22].

4.1.3. Mathematical model particularised for the physical piezoelectric harvester

For the first resonant frequency, a vibrating cantilever beam structure can be regarded as a mass-spring-damper system, having the same behaviour. For cantilever structures, the expression of the fundamental frequency is the following [24]:

$$f_n = \frac{1}{2\pi}\sqrt{\frac{k}{m_{eff}}} \tag{4.2}$$

where: f_n [Hz] – natural frequency; k [N/m] – stiffness constant; m_{eff} [kg] – effective mass.

Relying on the materials' moduli of elasticity [22] and on layer thicknesses, the cross-sectional stiffness K is calculated in (4.3) for the 17 layers of Midé PPA-4011.

$$K = b \cdot \left[\sum_{i=1}^{17} Y^{(i)} h^{(i)} \left(z_0^2 - z_0\left(H^{(i)} + H^{(i-1)}\right) + \frac{{H^{(i)}}^2 + {H^{(i-1)}}^2 + H^{(i)}H^{(i-1)}}{3}\right)\right] = 0.223 \ \frac{\text{kg}\cdot\text{m}^3}{\text{s}^2} \tag{4.3}$$

where: b [m] – Beam width; $Y^{(i)}$ [N/m^2] – Young's modulus for layer (i); $h^{(i)}$ [m] – thickness of layer (i); z_0 [m] – neutral axis coordinate; $H^{(i)} = \sum_{j=1}^{i} h^{(j)}$.

The coordinate z_0 of the neutral axis is calculated as:

$$z_0 = \frac{h_{total}}{2} = \frac{5 \cdot h_e + 8 \cdot h_s + 4 \cdot h_p}{2} = 0.62 \text{ mm} \tag{4.4}$$

where: h_e = 0.08 mm – FR4 thickness; h_p = 0.03 mm – Copper thickness; h_p = 0.15 mm – Piezo thickness.

Relying on the relation in [24], the first resonant frequency is calculated thus:

$$f_n = \frac{1}{2\pi} \cdot 1.875^2 \sqrt{\frac{K}{\rho_{equiv} \cdot A \cdot {L_{eff}}^4}} = 241.68 \text{ Hz} \quad (4.5)$$

where: ρ_{equiv} – equivalent density; A – beam surface area; L_{eff} [m] – effective length.

The equivalent density ρ_{equiv} from equation (4.5) above was calculated as 4469 kg/m^3. The piezoelectric cantilever is clamped in the rear clamp (Figure 12), the support's farthest position, enabling the maximum effective length subjected to vibrations, beneficial both due to a higher tip amplitude, as well as due to lower strain, which can lengthen the product lifetime.

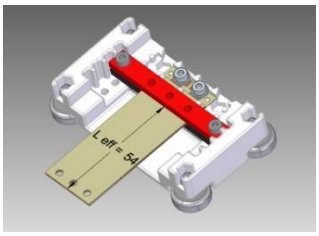

Figure 12. CAD model highlighting the effective length L_{eff} = 54 mm [9]

4.1.4. Equivalent circuit for the quadmorph piezoelectric harvester

Knowing that in the mechano-electrical analogy, the components have the following equivalences, the equivalent electromechanical circuit of a piezoelectric harvester can be represented by the resonant analogy type: inductance, L ⇔ mass, m; capacitance, C ⇔ compliance, or inverse of spring constant, $1/k$; resistance, R ⇔ damping, c. Figure 13 shows the electromechanical circuit of a piezoelectric transducer translated into electric domain.

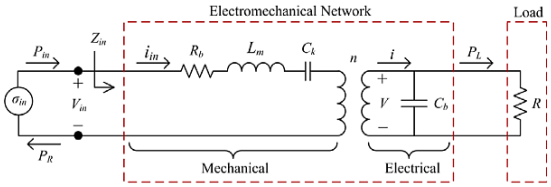

Figure 13. Electromechanical circuit of a piezoelectric transducer translated into electric domain [25]

The equivalent electric circuit of the physical quadmorph piezoelectric harvester presented and employed in the present thesis is schematized, according to the experimental tests, in Figure 14. The nodes numbering is used accordingly in the numerical simulations when declaring the electric circuit.

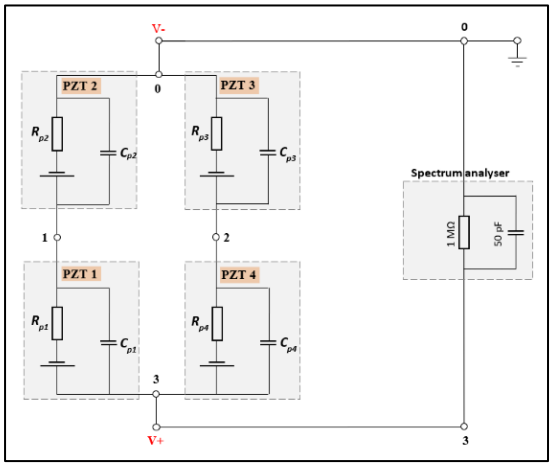

Figure 14. Equivalent experimental electric circuit

4.2. Digital twin of the piezoelectric harvester

Three-dimensional finite element models were developed and analysed in COMSOL Multiphysics (Figure 15), for predicting the piezoelectric harvester's behaviour. A Multiphysics approach is essential for analysing both mechanical aspects such as resonant frequencies, displacements, and von Mises stresses, and piezoelectric effect regarding electric output. Two intertwined physics are coupled for a Multiphysics evaluation of both mechanical and electrical parameters, namely ***Solid Mechanics*** and ***Electrostatics***. The two physics are interconnected through ***Multiphysics – Piezoelectric effect***. The electromechanical behaviour is assessed by coupling the following physics interfaces: ***Solid Mechanics***; ***Electrostatics***; ***Electrical circuit***.

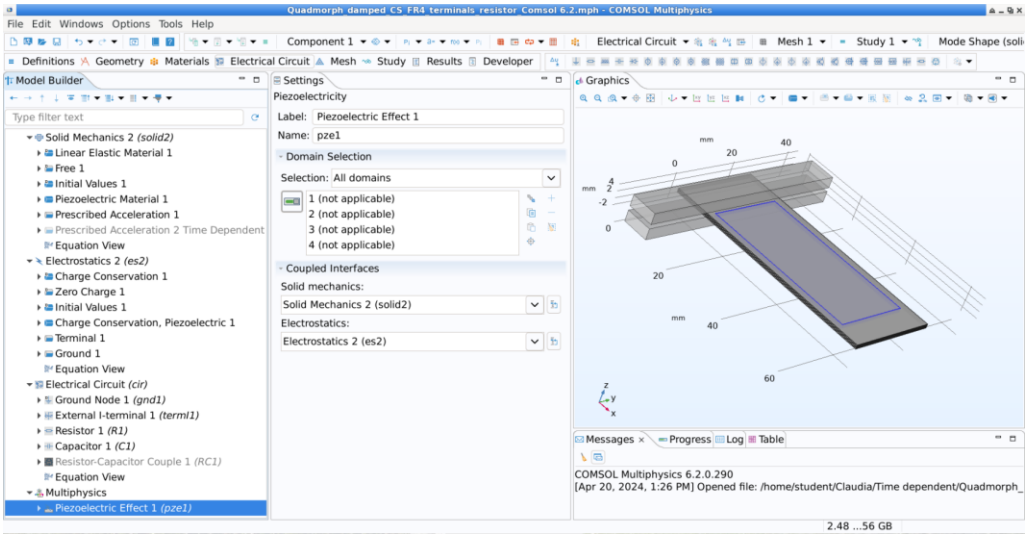

Figure 15. Fully coupled Multiphysics piezoelectric effect

4.2.1. Eigenfrequency study (modal analysis)

Eigenfrequencies, or ***natural frequencies***, are discrete frequencies at which a system is prone to vibrate. An ***eigenmode*** is the shape that a structure deforms into, which corresponds to vibrating at a specific eigenfrequency. The eigenfrequency study can only provide information about the shape of the mode. In Figure 16, the first 10 eigenfrequencies were extracted from the modal analysis study conducted.

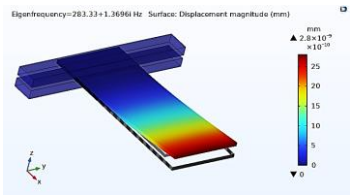

a) First bending mode

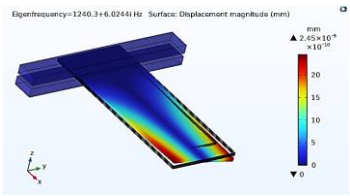

b) First torsional mode

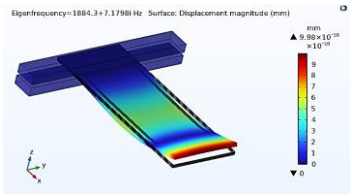

c) Second bending mode

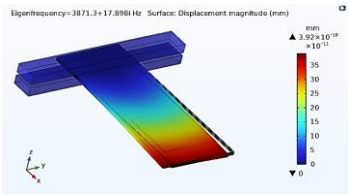

d) Bending in horizontal plane

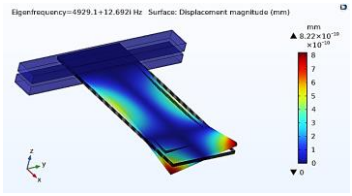

e) Second torsional mode

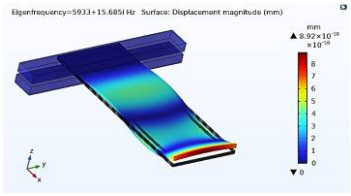

f) Third bending mode

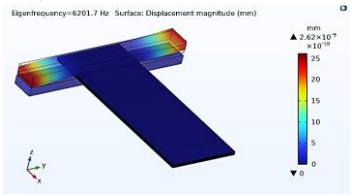

g) Clamping bar bent up and down

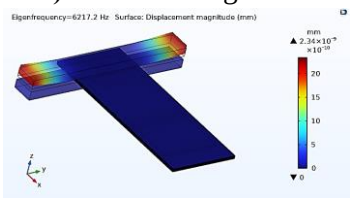

h) Clamping bar's both ends bent up

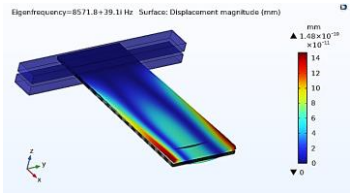

i) Bending mode in yOz plane

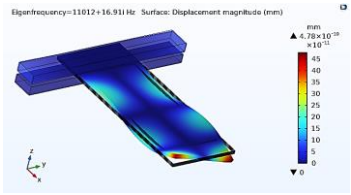

j) Combination of third bending mode with first torsional mode

Figure 16. First 10 vibration modes of the digital twin of Midé PPA-4011

4.2.2. Frequency Domain study

In solid mechanics, Frequency Domain study is used to compute the frequency response of a mechanical structure with respect to load distributions and frequencies. The voltage response obtained for [range(173,10,273) range(273,1,283) range(283,0.1,285) range(285,1,295) range(295,10,395)] is presented in Figure 17.

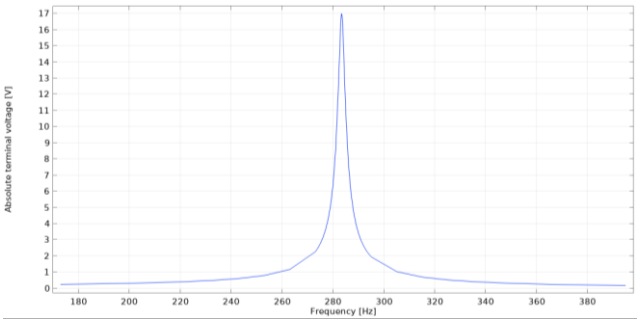

Figure 17. Frequency response function

4.2.3. Time Dependent study

The Time Dependent study and study step are used when field variables change over time. For example, in solid mechanics it is used to compute the time-varying deformation and motion of solids subjected to transient loads in the time domain [26]. The quadmorph structure renders an alternating voltage response, as shown in the captures from the numerical simulation in Figure 18, within a time range(0, Tp*0.05, Tp*140). The period time, Tp, was calculated as 1/fn, where fn is the first eigenfrequency.

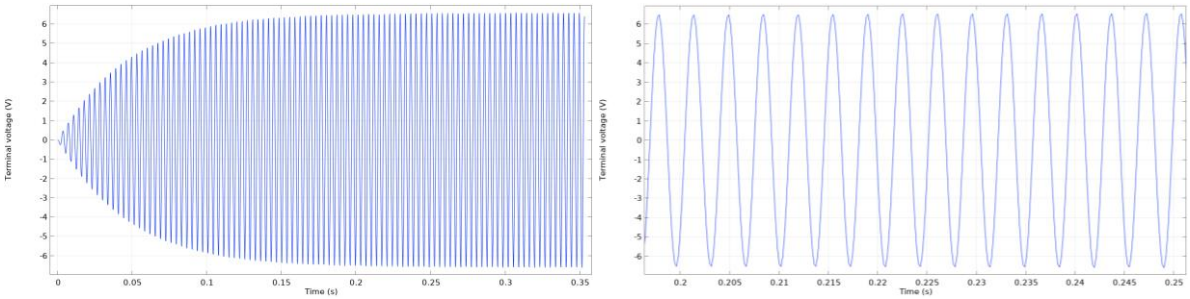

Figure 18. Sinusoidal response of the quadmorph piezoelectric cantilever (left) and zoom in (right)

4.3. Experimental laboratory tests

4.3.1. Laboratory setup

The ideal clamping location was established within the simulation to be the rear clamping position. The experimental setup in Figure 19 consists of:

- Dynamic ***spectrum analyser*** (Stanford SR785) with FFT capabilities and functions generator for driving the shaker, for frequency and voltage responses display and DAQ.
- ***Power amplifier*** (TIRA BAA 120) with sine output power of RMS value 120 VA, used for amplifying the driving signal from the analyser to the shaker table.
- ***Electrodynamic shaker table*** (TIRA S 513), controlled by the spectrum analyser via the power amplifier, being connected to the analyser's output channel.
- ***Piezoelectric energy harvester*** (Midé PPA-4011) fastened on the clamping support (Midé PPA-9001 clamp kit). The PEH is connected to input channel 2 of the analyser.
- ***Accelerometer*** (Brüel&Kjær 4507-B-006), connected to input channel 1 of the analyser. ICP type power supply was activated for this channel.

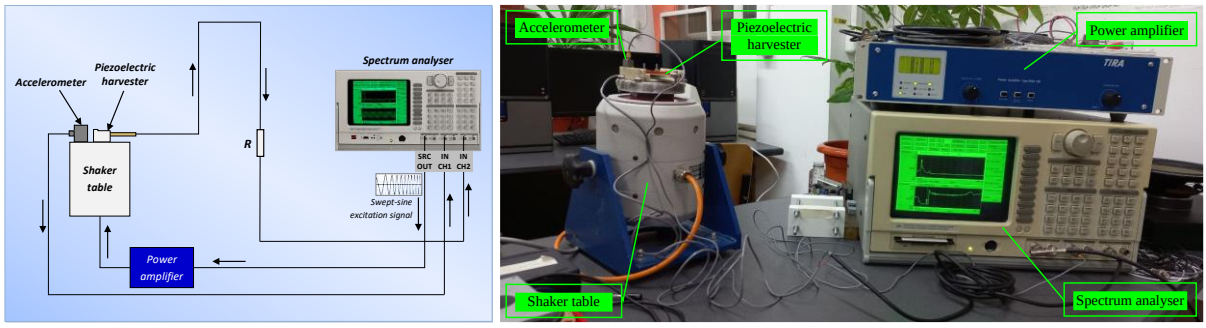

Figure 19. Block diagram and laboratory setup

4.3.2. Frequency response with swept-sine function

Swept-sine is a technique employed for characterising the frequency response of a tested device [27]. A stepping swept-sine (logarithmic) excitation signal, prescribed acceleration with constant amplitude, is applied to the shaker, varying the frequency in steps, within a frequency range.

4.3.3. Time response on the spectrum analyser

The time response displayed on the spectrum analyser's screen in Figure 20 shows the sinusoidal alternating voltage specific to a piezoelectric device subjected to imposed harmonic motion and forced vibrations.

Figure 20. Experimental tests displaying the sinusoidal time response

4.4. Boosting the electric output with an optimally shaped inertial mass

4.4.1. Piezoelectric harvester with no additional tip mass

The configuration of the first set of tests was with free tip. The voltage peak response with no tip mass is V_0 = 334.5 mV/(m/s^2), at a resonant frequency of 214.03 Hz (Figure 21).

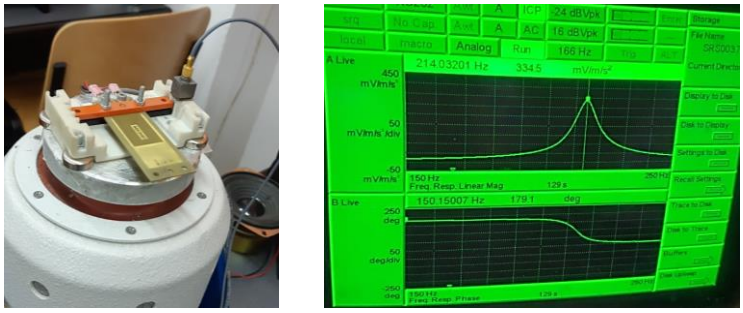

Figure 21. Tests with no additional tip mass and analyser displaying the voltage response

4.4.2. Piezoelectric cantilever with concentrated inertial mass

The configuration with concentrated mass rendered a voltage peak of 776.1 mV/(m/s^2), with 4 g mass, recorded in Figure 22, accompanied by a resonant frequency decrease, down to ~108.38 Hz. The percentage increase compared to free tip configuration is **132%**.

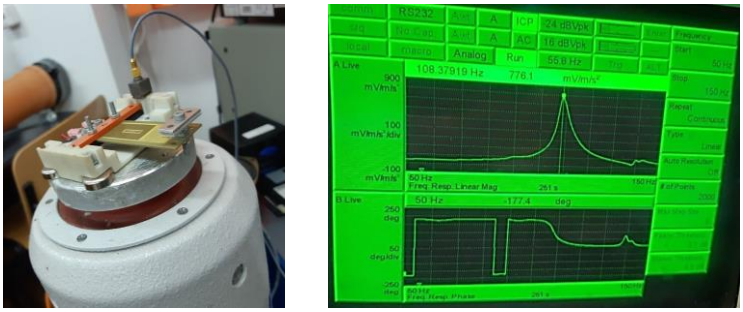

Figure 22. Piezoelectric beam with concentrated tip mass and voltage response display

4.4.3. Piezoelectric cantilever with tip curvature constraining elements

The most interesting case, with tip mass constraining the curvature in transversal vertical plane, recorded a maximum voltage of 836.7 mV/(m/s^2), at resonance of ~110.58 Hz (Figure 23). Blocking tip curvature on transversal plane increases the electric potential response, from the free tip case, with **~150%**. The frequency increases slightly with constraining tip mass of same value, due to adding thickness to beam cross-section.

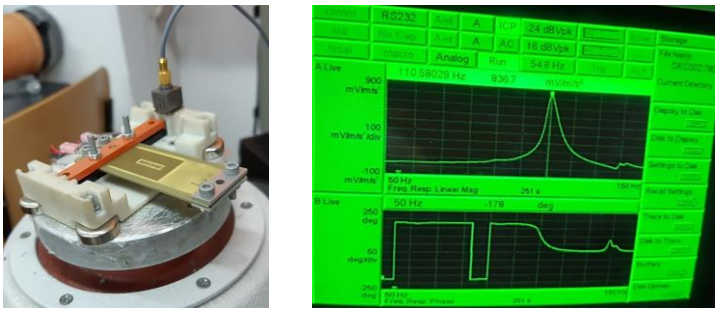

Figure 23. Piezoelectric harvester with constrained tip curvature

4.4.4. Experimental results

The data acquired from analyser is plotted in Figure 24. The free tip peak voltage recorded is 3.28 V/*g*, at the resonant frequency of 214.03 Hz. When attaching the concentrated mass, the voltage output increased to 7.611 V/*g*, at the resonance frequency of ~108.38 Hz. Constraining the tip curvature with blocking elements induces higher von Mises stresses into the beam's piezoelectric material, obstructing the corners to bend upwards and downwards in vertical plane. A voltage increase is recorded, along with a slight increase of the resonant frequency, found at 110.58 Hz. The voltage peak at resonance is 8.205 V/*g*.

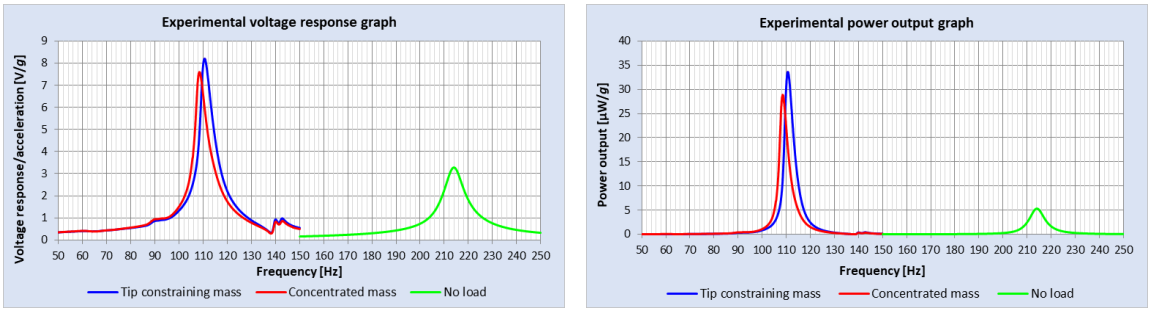

Figure 24. Voltage and power responses plots relying on acquired data

4.5. Thermal influences on the piezoelectric harvester

Temperature may alter the piezoelectric response and transducers' performances. Despite the improved performances for energy harvesting of PZT-5H, a soft lead zirconate titanate piezoceramic, this material is very sensitive with temperature. Temperature influence has little been studied in the literature for piezoelectric energy harvesters vs. sensors and actuators, due less precise control required. The evaluated range in the simulations was from -30 °C to 100 °C, comprising the range measured on the compressor.

4.5.1. Temperature dependent piezoelectric constants

At Curie temperature, the piezoelectric crystal structure tends to relinquish the asymmetry and dipoles alignment. This will subsequently cause the material to lose its piezoelectric properties. The main material properties prone to be affected by temperature are: d_{31} charge/stress constant; g_{31} voltage/stress constant; Q_m mechanical Quality factor; K relative dielectric constant. Other properties may be also affected, such as the thermal expansion coefficient, α, electrical resistivity, ρ, and RC time constant, π,

4.5.2. Piezoelectric constants variations with temperature

The four formerly discussed piezoelectric constants, that are highly dependent on temperature and significantly influence the transducer's response, are presented together with their specified values at room temperature ($T_r \approx 23$ °C) [22]. Relying on the data provided by the manufacturer [28], the percent deviations of the temperature-dependent piezoelectric constants were calculated at different temperatures. The left plots in Figure 25 show the percent deviations and the right plots each constant value evolution with temperature.

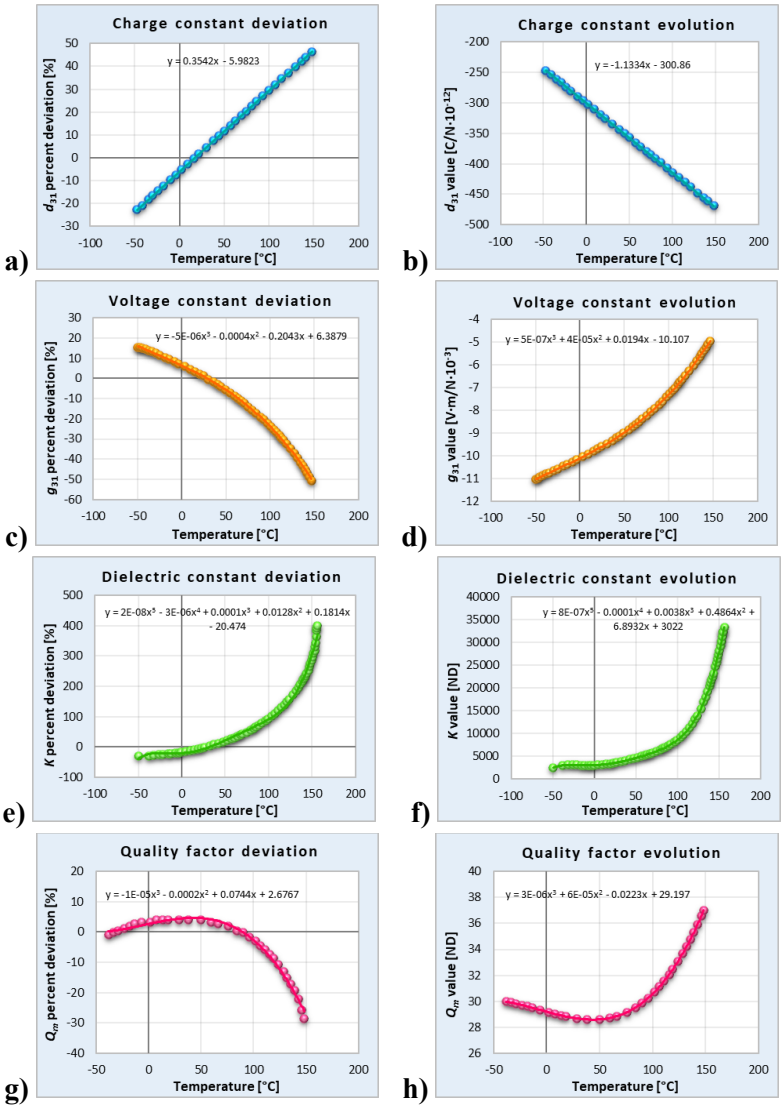

Figure 25. Piezoelectric constants percent deviations (left) and calculated values (right)

4.5.3. Free tip case (no inertial mass)

An eigenfrequency study was conducted beforehand (Figure 26), to establish the natural frequency value, and to define the frequency domain for finding the resonance peak. Mechanical damping was introduced, declaring an isotropic loss factor. The loss factor was calculated depending on each mechanical quality factor. Mechanical damping dominates in soft piezoceramic materials, rendering electrical damping negligeable.

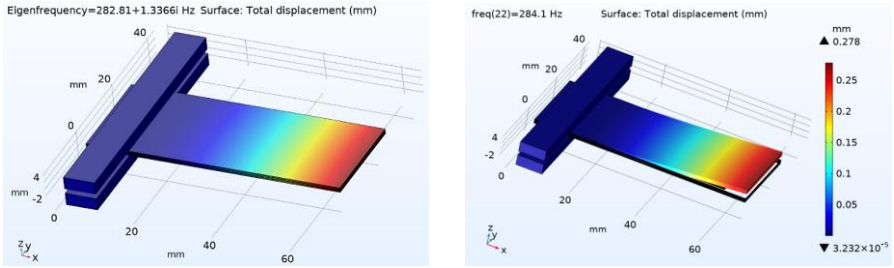

Figure 26. Free tip – First eigenfrequency (left); total displacement at resonance (right), at $T = 80$ °C

Figure 27 shows the electric potential distribution and von Mises stress evaluation within the piezoelectric beam. The detail shows how the terminals (V) and grounds (GND) were declared on the faces of the piezoelectric layers [22].

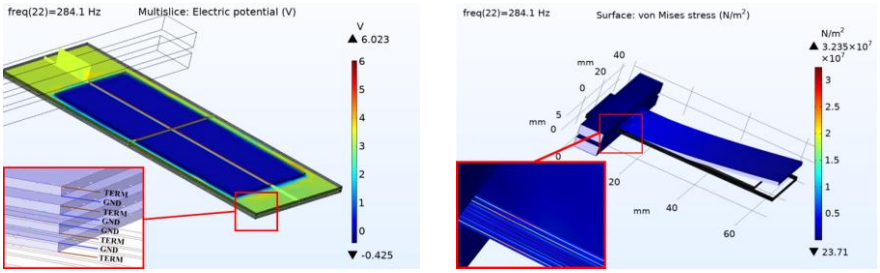

Figure 27. Free tip – electric potential (left) and von Mises stress (right), near resonance at $T = 80$ °C

The frequency response magnitude observed during laboratory tests on the upper channel of the signal analyser in Figure 28 is more attenuated than in the simulations. The analyser drives the shaker with a swept-sine signal, ensuring a time-harmonic mode.

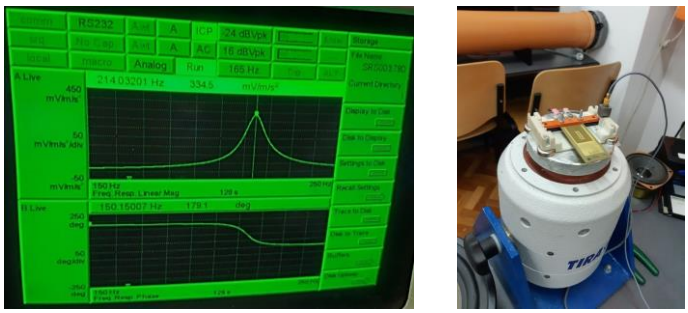

Figure 28. Voltage response on the spectrum analyser (left) and free tip PEH on shaker table (right)

4.5.4. Constrained tip case (with inertial mass)

The research herein also considers observing the behaviour of the piezoelectric cantilever with inertial mass in the form of constraining bars. Figure 29 shows the shows the von Mises stress evaluation, considering damping loss factor, and the electric potential distribution across the beam, near resonance f_r (< ±0.1 Hz).

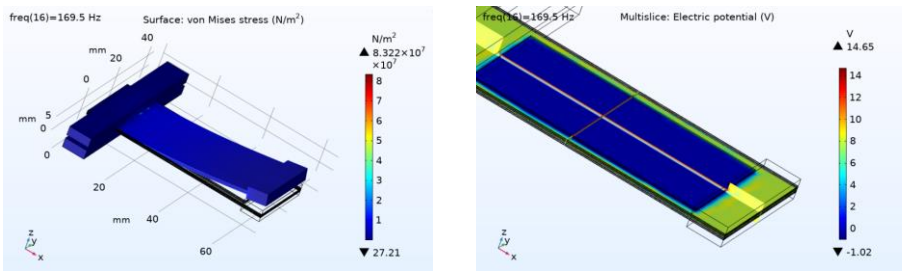

Figure 29. Constrained tip – von Mises stress (left) and voltage response (right) at $T = 80$ °C

4.5.5. Simulations results

The voltage sensitivity at resonance with respect to the working temperature, the resonant frequency, total displacement and von Mises stress are plotted in Figure 30. Even though the ***displacement increases with temperature***, the ***voltage response actually decreases***. The results obtained in the numerical simulations represent a very good indicator of optimal operation temperature conditions for a PZT-5H based piezoelectric. It is shown that its piezoelectric response is ***highly nonlinear***, and ***greatly affected by the operating temperature***.

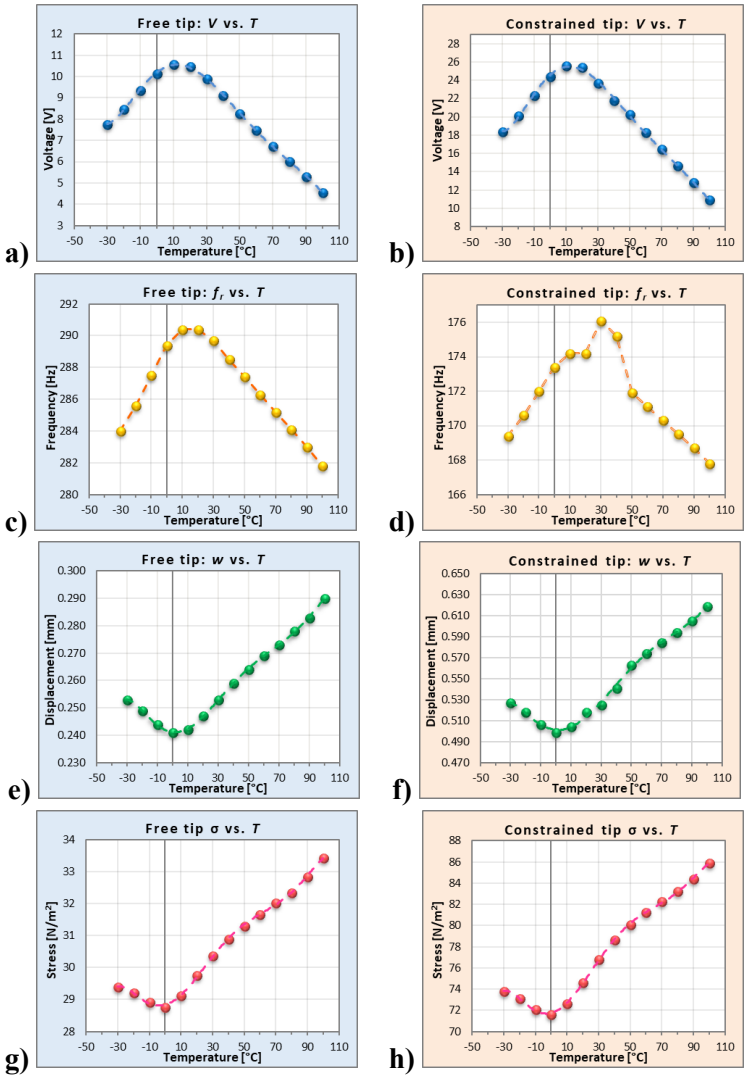

Figure 30. Voltage response: **a)** free tip, **b)** constrained tip; Resonant frequency: **c)** free, **d)** constrained; Total displacement: **e)** free, **f)** constrained; Von Mises stress: **g)** free, **h)** constrained

4.6. Shape optimization of the piezoelectric harvester towards triangular section

The idea of triangular longitudinal section for the cantilever has been considered, as an original research element [29], [30]. A comprehensive literature survey [29] shows that these studies are an original approach and have not been addressed in published literature so far.

The piezoelectric cantilever was simulated starting from rectangular to triangular, via three intermediate trapezoidal sections. A second study, which has not been approached in the literature before, aimed to assess the piezoelectric response on unit volume of piezoelectric material, thus proving an incontestable effectiveness of the fixed constrained material, considering a 4 g inertial mass. A third study, another novelty element, evaluates the mechanical stress. Attention was paid to keeping the mechanical stress to same value for all structures.

The five structures for the shape optimization analysis started from the digital twin model of Midé PPA-4011 rectangular cantilever. The length of the beams was not changed, being the same as for the rectangular one. The piezoelectric layers' fixed constrained cross-section was unaltered. Figure 31 shows the simulated shapes: **a)** rectangular; **b)** trapezoidal (wide tip); **c)** trapezoidal (medium tip); **d)** trapezoidal (narrow tip); **e)** triangular.

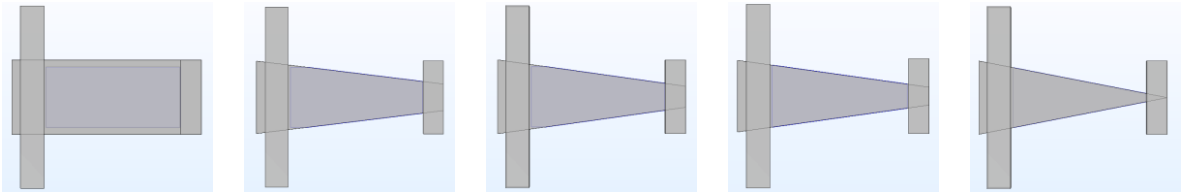

a) 143.52 mm^3, reference | **b)** 114.43 mm^3, -20.3% | **c)** 108.43 mm^3, -24.4% | **d)** 100.7 mm^3, -29.8% | **e)** 81.659 mm^3, -43.1%

Figure 31. The five structures and afferent material reductions in percents: **a)** rectangular (reference); **b)** trapezoidal, -20.3%; **c)** trapezoidal, -24.4%; **d)** trapezoidal, -29.8%; **e)** triangular, -43.1% [29]

The 3D model of the piezoelectric harvesting system employed in laboratory was designed (Figure 32), employing a tip mass of 4.0 g at the free tip, as well as the clamping support for the fixed constraint of the cantilever between two bars at the other end.

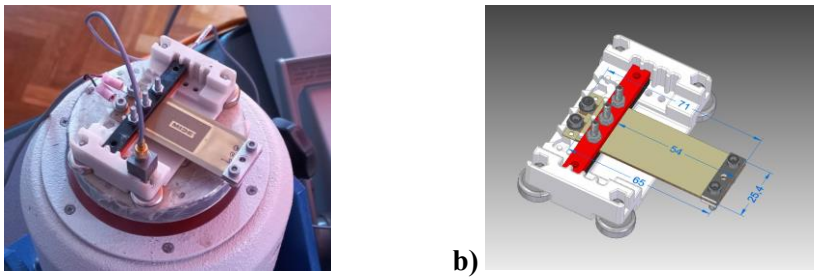

a) **b)**

Figure 32. a) Experimental PEH system on shaker table and **b)** 3D CAD model designed [29]

When an electric circuit is added in the simulation model, consisting of a 1 MΩ || 50 pF resistor-capacitor couple [31], [32], von Mises stress is reduced, from 80.06 MPa in no load, to 78.5 MPa due to resistor's dissipative nature, employed further in the study under same stress.

4.6.1. Material cutoff maintaining the same inertial mass

First, the five structures were analysed maintaining the inertial mass value of 4 g as in the laboratory experiments. The tip mass and its constraining shape were set so as to resemble

the experimental setup [31]. The inertial mass was calculated based on the default density of structural steel in the simulation program, $\rho = 7866$ kg/m^3. The length and width of the two bars respect the physical dimensions, $L \cong 25.4$ mm and $W \cong 7$ mm. The triangular electric potential runs about 13% lower, along with reducing more than 43% of active piezoelectric material (Figure 33). This is enough to prove that the fixed constrained material is more effective.

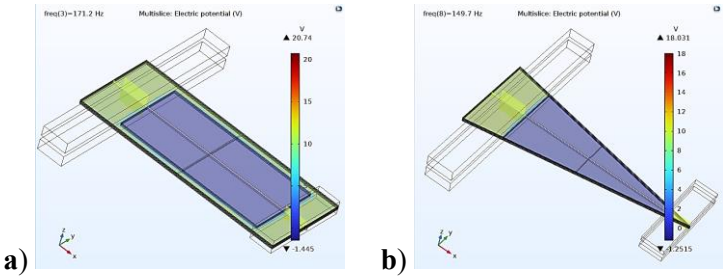

Figure 33. Electric potential for: **a)** rectangular structure, **(b)** triangular structure

The triangular case records a decrease down to almost a third of the stress computed for the rectangular cantilever, as one can see in Figure 34. In triangular case with same inertial mass, displacement is slightly lower due to a higher compliance.

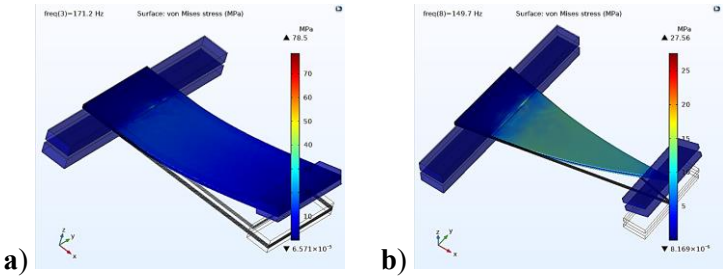

Figure 34. Mechanical stress at resonance for: **a)** rectangular and **b)** triangular structures

Figure 35 plots similar voltage and active power trends, and the total displacement. The values from horizontal axes are reversed, for an easier grasp of the stress decrease with ~65% towards triangular case. Voltage increases with ~53% per unit volume, from rectangular to triangular and the power per unit volume increases with 30.4% (Figure 36).

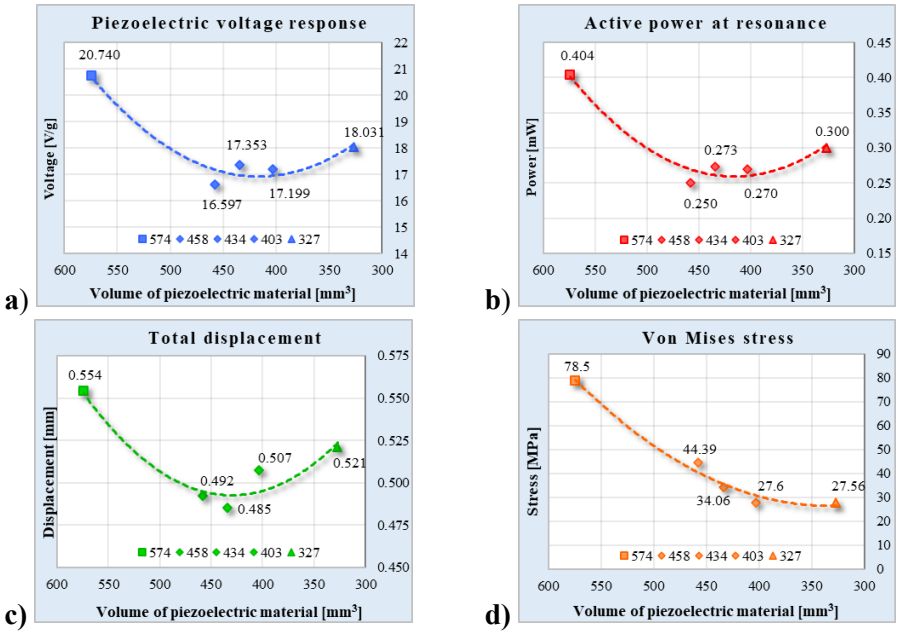

Figure 35. a) Voltage response, **b)** Active power, **c)** Total displacement, **d)** von Mises stress

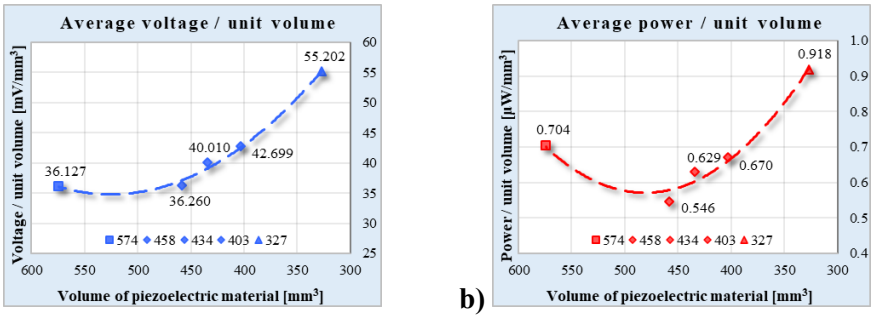

a) b)

Figure 36. a) Average voltage, **b)** Average power [with same inertial mass, per unit volume]

4.6.2. Material cutoff maintaining same mechanical stress

Observing how the mechanical stress decreases, it was interesting to conduct a second set of simulations maintaining same stress. Several simulations had to be performed as stress is not linear with tip mass and depends on beam's geometry. Figure 37 reveals that an over 2.5 times higher voltage and an almost 6.4 times more power is obtained with the triangular shape, displacement is ~3 times higher in same stress conditions, and the inertial mass supported is ~3.3 times larger than for rectangular case. The increase in voltage per unit volume with ~342% and power per unit volume with 1022% are outstanding for the triangular structure (Figure 38).

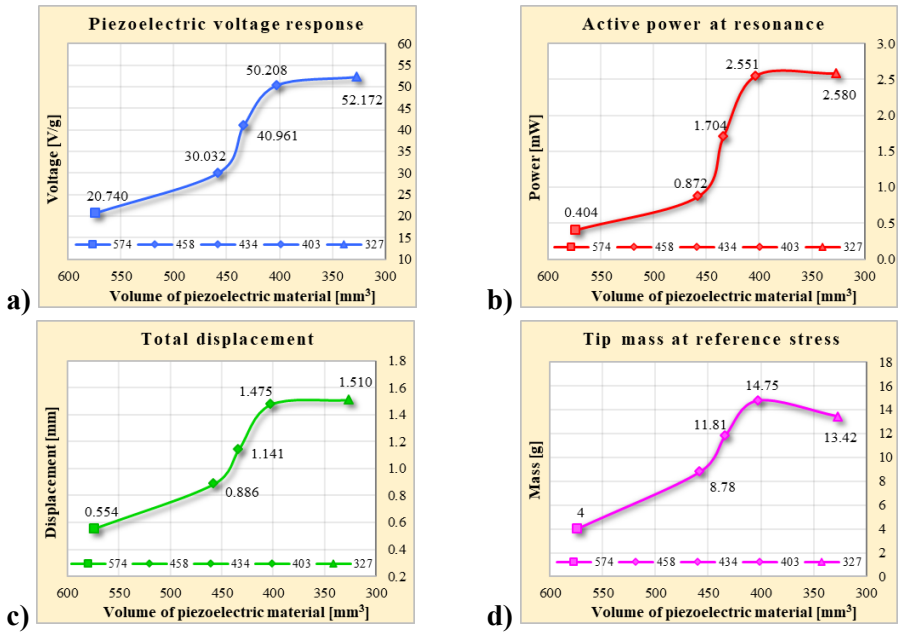

a) b) c) d)

Figure 37. a) Voltage output, **b)** Power output, **c)** Total displacement, **d)** Inertial mass for 78.5 MPa

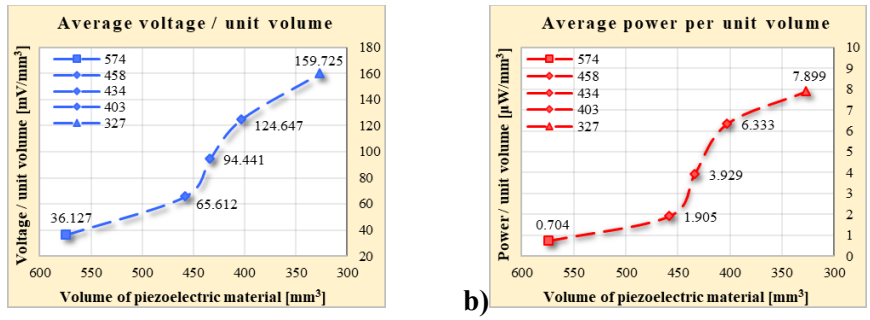

a) b)

Figure 38. a) Average voltage and **b)** Average power [per unit volume **at same stress**]

4.7. Optimal resistive load for maximizing piezoelectric power output

The matching load was assessed for three cases: rectangular cantilever, triangular cantilever with same mass of 4 g, and triangular cantilever under same stress of 78.5 MPa. Figure 39 shows that the resistance for maximum power is almost two orders of magnitude lower than the spectrum analyser's resistance of 1 MΩ.

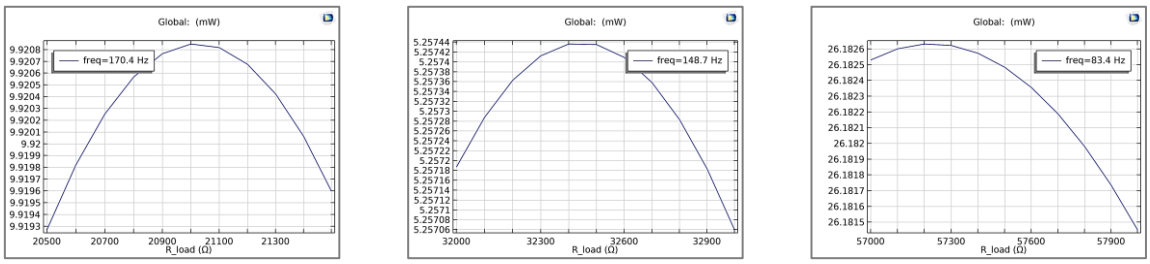

a) Rectangular **b**) Triangular, same mass **c**) Triangular, same stress

Figure 39. Load dependence curves for the three structures assessed

Table 3 summarizes the results. The maximum power outputs for matched resistance (P_{MAX_opt}) increase tremendously compared to simulations where 1 MΩ || 50 pF impedance was used (P_{RMS_max}), namely: ~1145% increase for the rectangular structure, ~724% for triangular structure with the same mass, and ~389% increase for triangular structure under the same stress.

Table 3. Simulation results for optimal resistive load for maximum power output

No.	Cantilever section (Vol_{piezo_layer})	Vol_{piezo_total} [mm³]	m_i [g]	ρ_i [kg/m³]	f_r [Hz]	f_{P_max} [Hz]	P_{a_max} [mW]	R_{load_opt} [kΩ]	P_{MAX_opt} [mW]	$V_{P\_max\_abs}$ [V]	k_{eff} [ND]
1	Rectangular, (143.52 mm³)	574.08	4	7866	171.2	170.4	0.797	21.0	9.921	20.413	0.27053
2	Triangular, same mass (81.659 mm³)	326.64	4	7866	149.7	148.7	0.638	32.4	5.257	35.715	0.26731
3	Triangular, same stress (81.659 mm³)	326.64	13.42	26400	84	83.4	5.358	57.2	26.183	54.777	0.26958

The piezoelectric response was optimised within a load dependence frequency domain study, by adding an auxiliary sweep of the load resistance, *R_load*. The maximum power boost was obtained with a 21 kΩ resistor, at the frequency of 170.3 Hz (Table 4).

Table 4. Simulation results

Frequency domain study	Resistor *R_load*	Capacitor	f_r [Hz]	f_{P_max} [Hz]	abs(*cir.RC1_rcr_v*) [V]	P_{max} @f_{P_max} [mW]
Frequency domain, range(170,0.1,172) Hz	1 MΩ	50 pF	171.2	170.4	39.927	0.797
Load dependence, range(170.2,0.1,171.2) Hz, auxiliary sweep, *R_load*, range(10,1,50) kΩ	Optimal: 21 kΩ	50 pF	171.2	170.3	20.466	9.973

5. THERMOELECTRICITY

Thermoelectricity is the direct conversion of temperature gradient into electricity or, inversely, electricity into heat through two related phenomena, namely Seebeck effect and Peltier effect. Traditionally, *thermoelectricity* encompasses three phenomena, namely *Seebeck*, *Peltier* and *Thomson effects*. Even though they are inverse phenomena (similarly to direct piezoelectric effect vs. inverse piezoelectric effect), separation of Seebeck and Peltier effects is a consequence of their independent discoveries by two separate physicists.

5.1. Thermoelectric effects

Thermoelectric effect refers to the conversion into electric energy from a thermal gradient (Seebeck effect), and inversely, producing thermal energy (heating or cooling) from electric energy (Peltier effect). A third thermoelectric phenomenon, called Thomson effect, relates the other two together. The observed phenomena are:

- ***Seebeck effect***, supposing generation of a voltage produced by a heat flow, at the interface of two dissimilar electric conductors, with different Seebeck coefficients.
- ***Peltier effect.*** Refers to heating or cooling the system when a charge current *Ic* flows through the interface.
- ***Thomson effect***. Thomson effect is the amount of heat transported by a moving charge (electron) per unit of temperature increase across a material.

5.2. Brief history and principles of thermoelectric energy harvesting

The beginning of thermoelectric observations leads back to the end of 18th century. In year 1794, the Italian physicist Allesandro Volta made a noteworthy and very interesting observation, that a metal rod with a temperature difference between its ends caused a spasm in a frog's muscles. With today's knowledge, this is explained by the temperature difference in the metal rod gave birth to an electric current, exciting the muscle. At that time, it remained unexplained until 1822, when Thomas Seebeck rediscovered same effect while observing that a compass needle deflects in the vicinity of two metals junctions maintained under different temperatures [33]. The direct conversion into electricity from temperature gradient at the junction of two dissimilar conductors is known as the Seebeck effect. Altogether, ***Seebeck effect***, ***Peltier effect*** and ***Thomson effect*** describe today's thermoelectricity principles.

5.3. Thermoelectric generators

Thermoelectric generators are being considered a feasible solution for energy harvesting applications from the industrial processes' waste heat. Thermoelectric devices can harness this waste heat by converting temperature differences (or gradients) into electric energy. For an increased conversion efficiency, thermoelectric materials need to have both a high

electrical conductivity and low thermal conductivity at the same time. Thermoelectric generators (Figure 40) principle of operation is based on Seebeck effect. A module's thermocouples are electrically connected in series, by copper bridges, and thermally in parallel.

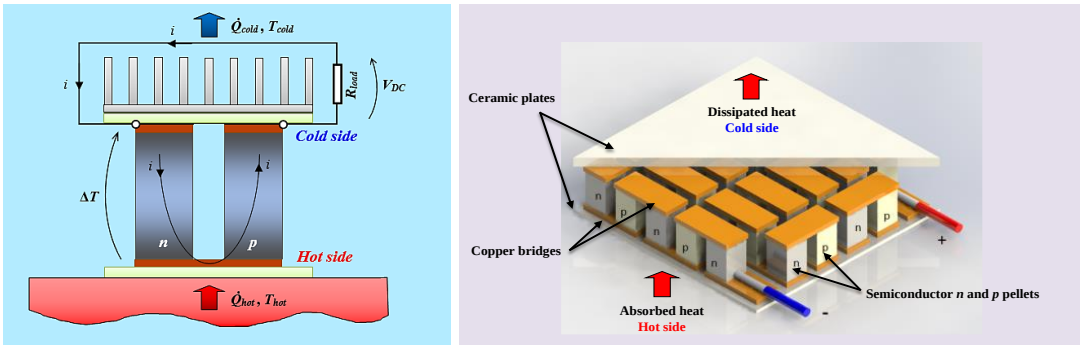

Figure 40. Operation principle of thermoelectric generator (left) and CAD model of TEM [34] (right)

5.4. Constitutive relations of thermoelectric materials

In a thermoelectric device, the main occurring phenomena are the thermoelectric effects, namely Seebeck, Peltier and Thomson effects, accompanied by Joule heating. Seebeck effect is the useful one for energy conversion from temperature gradient to electric energy.

The thermoelectric conversion efficiency of a TEG is calculated as ratio between the electric output power and the heat input rate absorbed at the thermoelectric generator's hot junction, written as (5.1). TEGs efficiency depends on temperature difference ($\Delta T = T_h - T_c$) across the module and cannot exceed Carnot efficiency.

$$\eta_{\mathrm{TEG}} = \frac{P}{\dot{Q}_h} \Rightarrow \eta_{\mathrm{TEG}} = \frac{R_L I^2}{\dot{Q}_h} \tag{5.1}$$

where: η_{TEG} [%] – thermoelectric generator efficiency; P [kWh] – electric power; $\dot{Q}_h$ [J] – heat rate (thermal power); R_L [Ω] – external load resistance; I [A] – electric current.

The efficiency of a thermoelectric device is related to the material's *figure of merit* (zT), dependent on its transport properties, according to relation (5.2).

$$zT = \frac{\varepsilon^2 \cdot \sigma \cdot T}{k} \Rightarrow z = \frac{\varepsilon^2 \cdot \sigma}{k} \tag{5.2}$$

where: zT [ND] – thermoelectric figure of merit; ε [V/K] – Seebeck coefficient; σ [1/Ωm] – electrical conductivity; k [W/mK] – thermal conductivity; T [K] – temperature.

5.5. Finite element method simulations with a single n-p thermocouple

A CAD model (Figure 41 left) was designed according to a reference model [35], [36] to show the dimensions of simulated thermocouple. The boundary conditions are pictured in Figure 41 right. The hot side planar surface is variated from 70 °C to 120 °C in a parametric sweep stationary study. The temperature of the cold side planar surface is set to be 30 °C. In TEG modules, p-type and n-type thermoelectric pairs are connected electrically in series and thermally in parallel. The end of the n-type leg is defined as Floating Potential and the other

end, from the p-type leg is defined as Ground. A stationary study was conducted, with a parametric sweep of the hot side of (70, 1, 120) degC, and the cold side set at 30 degC.

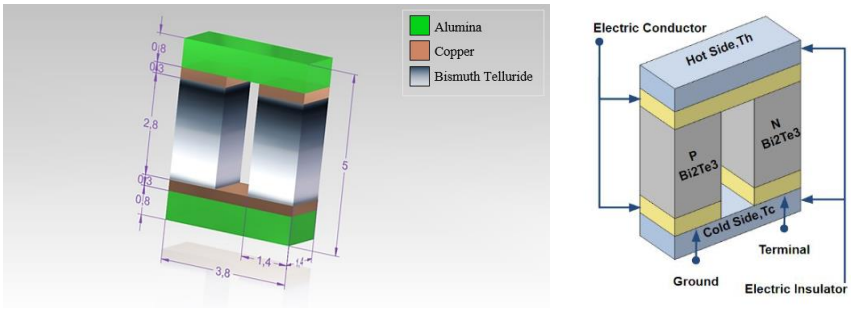

Figure 41. CAD model with the dimensions of TEG geometry (left) and boundary conditions (right)

The n-type semiconductor leg is selected in Figure 42, for which the Seebeck coefficient is set with negative sign, unlike the p-type leg.

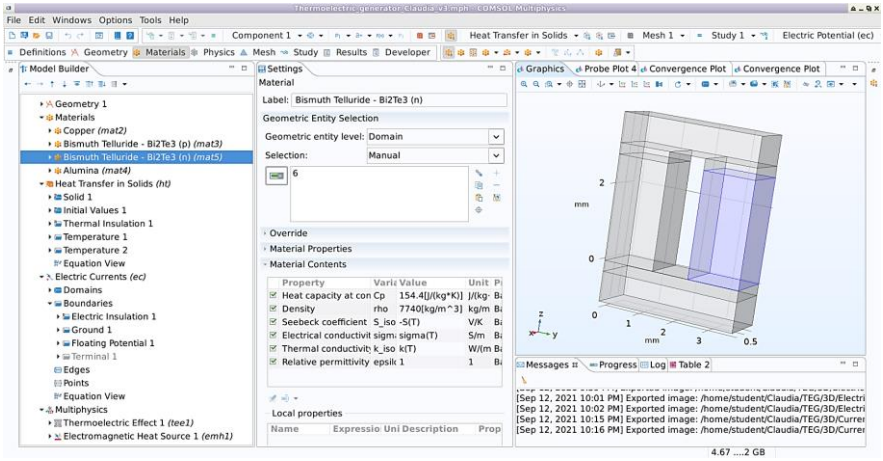

Figure 42. FEM program simulation interface and TEG geometry (Bi_2Te_3 elements selected)

The FEM simulations were conducted using a Multiphysics approach, for a complete evaluation of both heat transfer problem and electric field problem. This was realised by interconnecting two physics through ***Thermoelectric Effect*** Multiphysics approach, namely:

- ***Heat Transfer in Solids***.
- ***Electric Currents***.
- ***Thermoelectric Effect*** Multiphysics interface.
- ***Electromagnetic Heating*** Multiphysics interface.

The temperature distribution is shown in Figure 43, along with the total heat flux direction, highlighted by the red arrows. The electric potential has a maximum of 19.62 mV for a temperature difference of 90 °C between T_h = 120 °C and T_c = 30 °C.

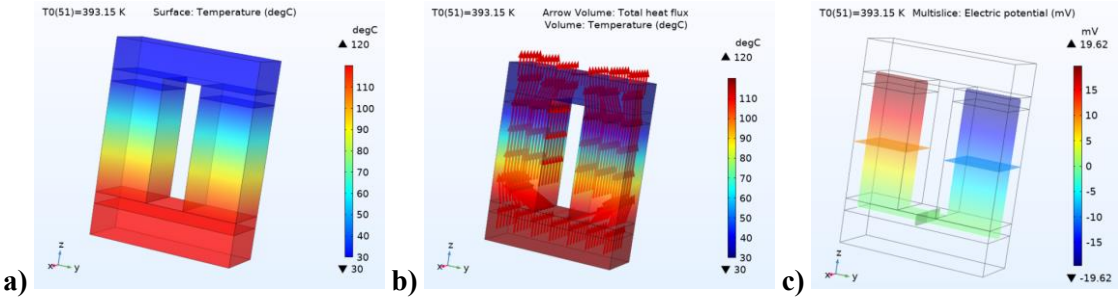

Figure 43. a) Surface temperature; **b)** Total heat flux; **c)** Electric potential, for hot side 120 °C

6. THERMOELECTRIC ENERGY HARVESTING SYSTEM PROPOSED

6.1. TEGpro TE-MOD-10W4V-40 thermoelectric generator

The thermoelectric part of the energy harvesting system proposed in this thesis consists of Bi_2Te_3 based thermoelectric modules. The TEGpro TE-MOD-10W4V-40 modules' overall dimensions are 40 mm x 40 mm x 5 mm (L x W x H). These ones can provide an output power of up to 6 W / 10 W and a voltage output of 4 VDC [37].

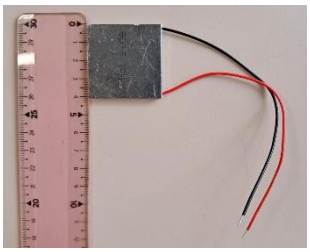

6.2. Digital twin of the physical thermoelectric module

6.2.1. Geometry and boundary conditions

The numerical model considers the specifications and overall dimensions of the real thermoelectric modules [37]. For numerical model's geometry, an intermediate number of 72 thermocouples was used. The geometry of the numerical model in Figure 44 was designed relying on a parametrized application builder [38], intended for thermoelectric coolers. The module's overall dimensions are according to datasheet [37], (L × W × H) 40 × 40 × 5 [mm].

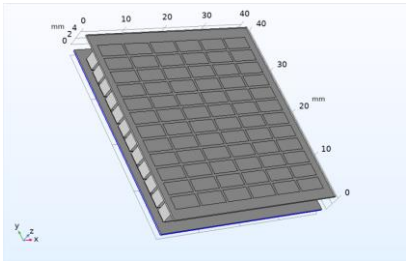

Figure 44. Thermoelectric model geometry

The FEM simulations employ a fully coupled Multiphysics approach [39], Bismuth telluride (Bi_2Te_3) was assigned for the thermoelectric legs of n-type and p-type, copper for the connection electrodes, and the hot side and cold side plates were considered of alumina ceramic.

The digital twin of the thermoelectric generator employs a full coupling of the following physics interfaces, for which the boundary and initial conditions are presented:

- ***Heat Transfer in Solids***. A Temperature 1 (T1) of 30 °C was declared for the cold side, and Temperature 2 (T2) of 80 °C was initially set for the hot side (Figure 45a).
- ***Electric Currents***. Ground (GND) and Floating Potential (FP) boundary conditions are applied on the surface in contact with the hot side plate, like in Figure 45b.

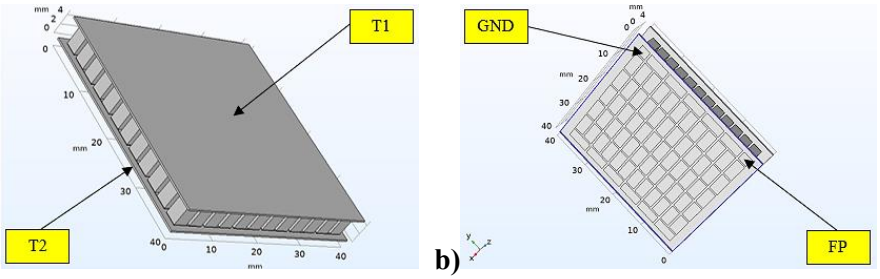

Figure 45. a) Boundary conditions applied in **a)** Heat Transfer in Solids and **b)** Electric Currents

- ***Thermoelectric Effect*** Multiphysics interface couples the physics interfaces Heat Transfer in Solids with Electric Currents for the complete modelling of the thermoelectric effects Peltier-Seebeck-Thomson [40].
- ***Electrical Circuit*** physics interface should be used if external circuit components ought to be added in the simulation. A 2.4 kΩ load resistor was connected in parallel.
- ***Solid Mechanics***, introduced to account for the triaxial vibrations of CU90G [41], [42].

6.3. Simulations with cold side and hot side temperature boundary conditions

6.3.1. Stationary study

The stationary study aims to assess the thermal and electrical parameters. A parametric sweep was considered for T_{hot}, within the range(40,5,80) °C. The temperature gradient across the TEG, from 30 °C to 80 °C, and the output in volts direct current (VDC) for Thot = 80 °C are presented in Figure 46.

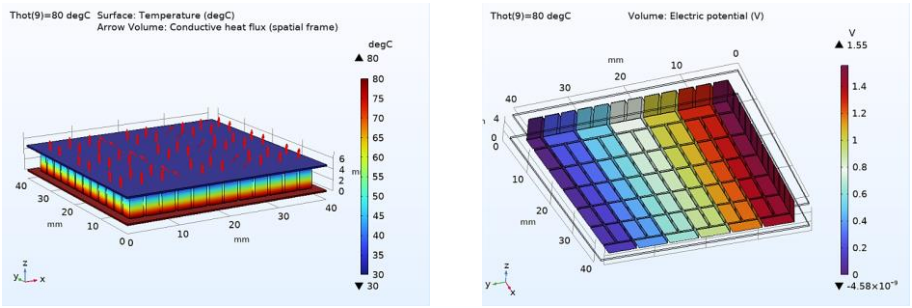

Figure 46. Temperature gradient across the TEG (left) and electric potential (right) for Thot = 80 °C

Figure 47 presents the voltage, current and power characteristics depending on the hot side temperature, plotted within the simulation program. The voltage across device is represented on the primary axis on the left side, while the secondary axis on the right side contains the values for current [mA] and power [mW] to device. The device is represented by the 2.4 kΩ load resistor considered. The linearity of the current-voltage dependency validates that the results obtained are correct, also confirmed by the as well as the current-power trend

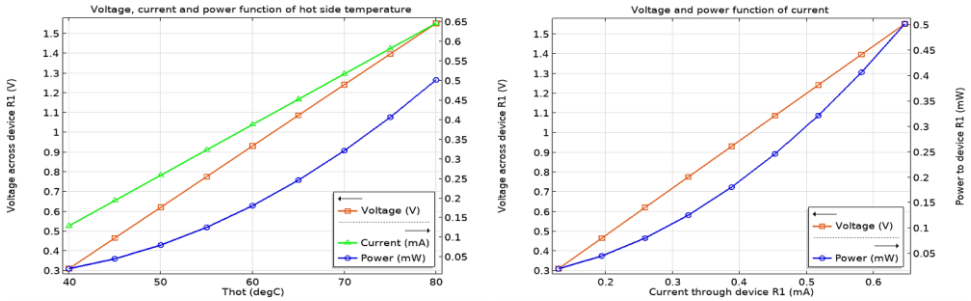

Figure 47. Voltage, current and power to device, depending on T_{hot} [12]

6.3.2. Structural frequency domain study

It was evaluated, through a frequency domain study, if the thermoelectric module is able to withstand the sinusoidal vibration of the compressor [12]. The maximum stress value of

0.759 kPa at 83.5 Hz that resulted in Figure 48 is negligible compared to the yield strength bismuth telluride material supporting compression stress values up to 62 MPa according to [43].

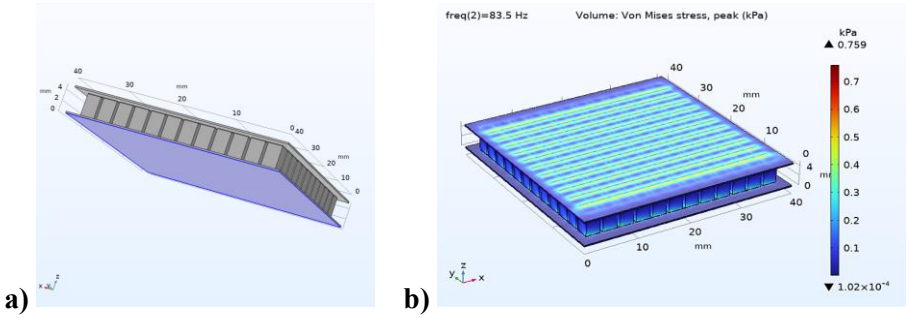

Figure 48. a) Boundary for prescribed velocities, **b)** Von Mises stress evaluation

6.4. Simulations considering heat flux, improving efficiency with a heatsink

The simulations employ a full coupling of Heat Transfer in Solids and Electric Currents, via Thermoelectric Effect Multiphysics interface [44], for a full modelling of the Peltier-Seebeck-Thomson effects altogether. Electromagnetic Heating is also coupled to account for resistive heating (Joule effect) [11].

The thermoelectric behaviour is assessed by interconnecting three physics:

- ***Heat Transfer in Solids*:** an initial hot side temperature, *Thot*, 100 degC is set, and a convective heat flux (natural convection with air at 1 atm, with external temperature of 20 degC) is set instead of *Tcold* used in previous set of simulations. For the model with heatsink in Figure 49, a thermal contact condition is added on TEG's cold side.
- ***Electric Currents*:** Ground and a Floating Potential type Circuit are declared on the faces of the terminal legs (see [11]).
- ***Electrical circuit*:** The node connections are declared: 0 – ground, and 1 – External I-terminal, applying the floating potential (ec/fp1) from Electric Currents, relative to ground. A load resistor of 2.4 kΩ is declared in parallel with the thermoelectric module.

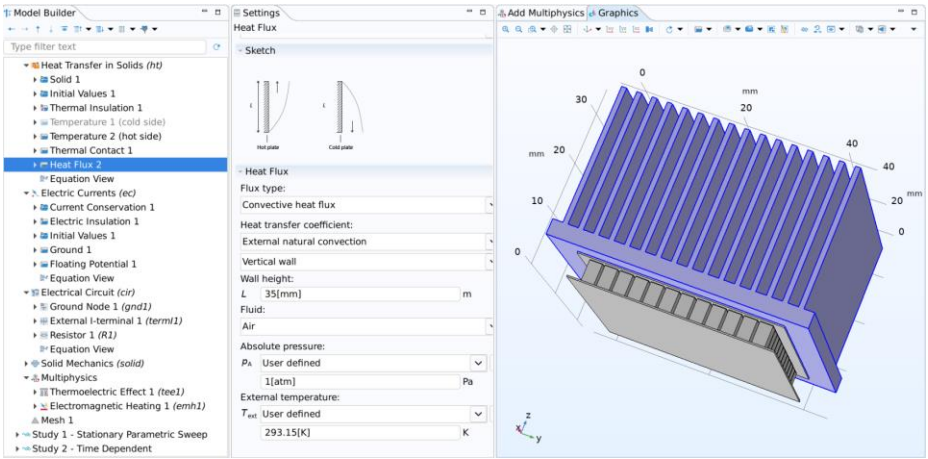

Figure 49. Simulation model with heatsink showing the Heat Flux boundary condition and settings

6.4.1. Stationary study

A stationary study with a parametric sweep of hot side temperature, *Thot*, range(30,5,100) degC, was conducted. The power computed [45] considers the voltage and current through resistor (*R1*), written as: 0.5*realdot(cir.R1_v, cir.R1_i). The plots in Figure 50a and Figure 50b outline the important differences between the TEG without heatsink and with heatsink. An improvement with one order of magnitude, in natural convection conditions, is achieved when using the heatsink. The voltage is 1.2 V with heatsink vs. 0.19 V without, current reaches ~0.3 mA vs. to 0.08 mA, and power reaches almost 0.3 mW vs. 0.008 mW.

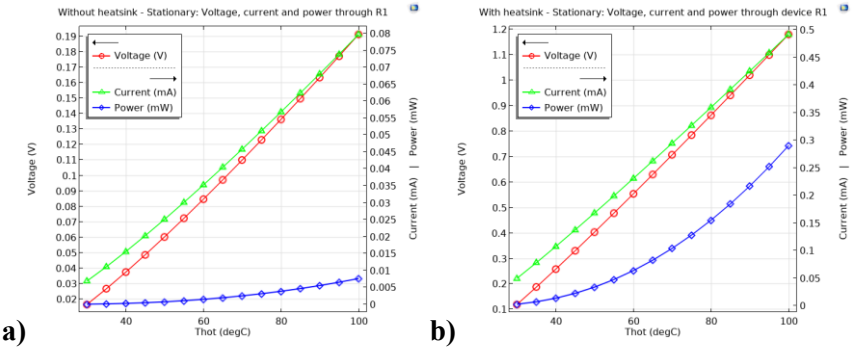

Figure 50. Stationary study – voltage, current and power: **a)** without heatsink, **b)** with heatsink

6.4.2. Time dependent study

It is worthwhile to see how the thermoelectric output behaves over time, and how fast it stabilizes thermally. A time dependent study, range(0,1,60) min was also run to see the thermal stabilization between hot and cold sides, with *Thot* = 100 degC. The graphs in Figure 51 offer extra information about the heatsink effect on the electrical parameters, these ones decreasing more smoothly and maintaining values with almost one order of magnitude higher than without heatsink. The Stationary study provides the values after thermal stabilization.

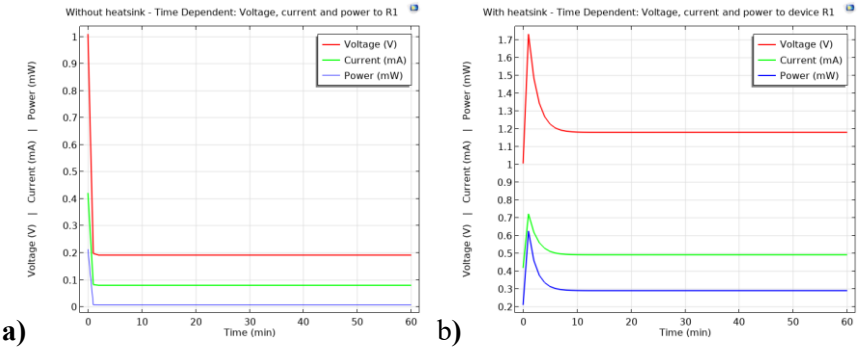

Figure 51. Time Dependent study – voltage, current and power: **a)** without heatsink, **b)** with heatsink

6.4.3. Structural frequency domain study

In the case without heatsink, the von Mises stress when declaring heat flux are slightly higher than when declaring certain temperatures for the hot side and for the cold side, namely 0.965 kPa compared to 0.759 kPa at the frequency of 83.5 Hz (see Figure 52a). For the validity of matching with the experimental conditions, the evaluation is more relevant for the model

with heatsink. Figure 52b shows a stress increase with more than one order of magnitude, reaching 14.1 kPa. This value, however, is still negligible compared to the yield strength of thermoelectric material used, which can withstand compression stress of up to 62 MPa.

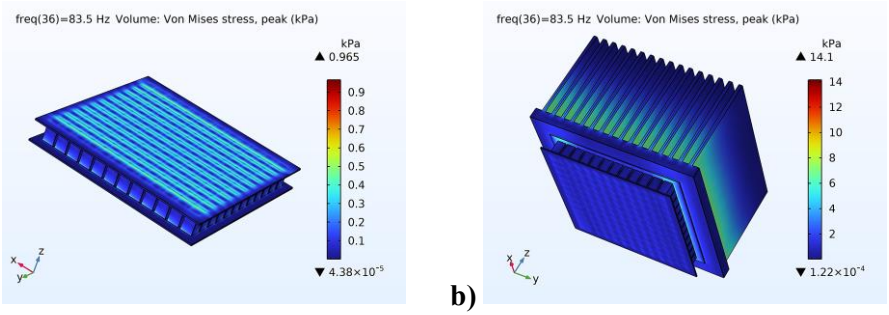

Figure 52. Von Mises stress evaluation **a)** without heatsink, **b)** with heatsink

7. EXPERIMENTAL TESTS WITH THE ENERGY HARVESTING SYSTEMS IN AN INDUSTRIALLY RELEVANT ENVIRONMENT

This section deals with the preliminary experimental validation in industrially relevant conditions, for both the piezoelectric and the thermoelectric energy harvesting methods addressed in this thesis. The experimental measuring setup for both the piezoelectric and thermoelectric energy harvesting systems is presented in Figure 53.

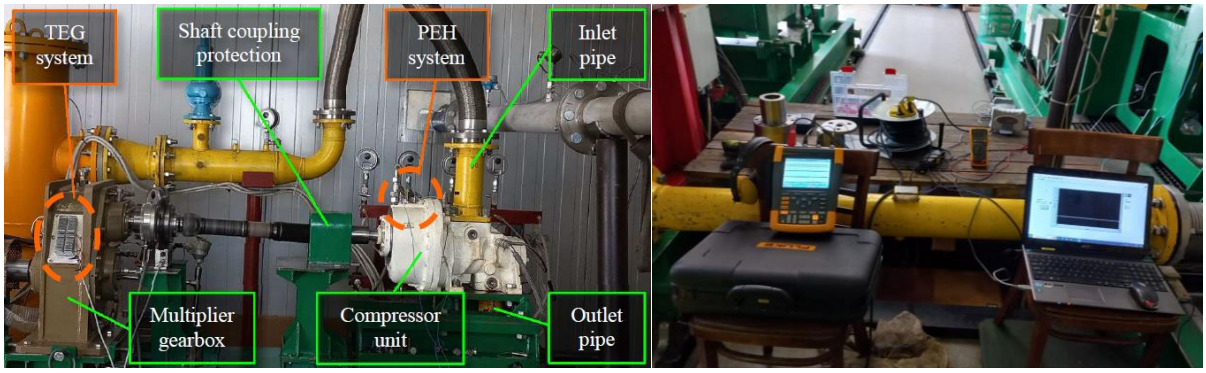

Figure 53. Compressor skid, at headquarters of INCDT COMOTI (left), Experimental setup (right)

The thermographic image in Figure 54 was taken during the experimental validation.

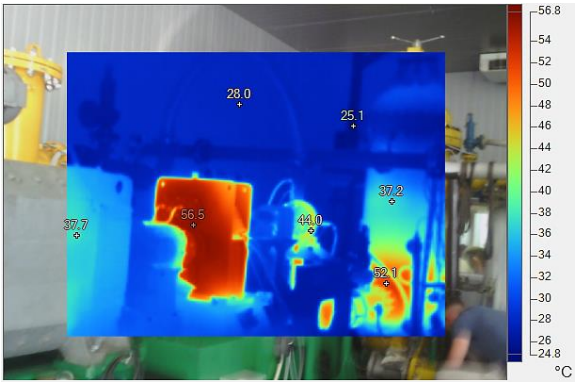

Figure 54. Thermographic image of the overall compressor skid

7.1. Piezoelectric system harvesting the vibrations of a rotary screw compressor

This work makes a step forward towards practical applications in industry (Figure 55), achieving a technology readiness level TRL 6 and demonstrating the technology in an industrially relevant environment [42]. The validation tests were conducted on **6th July 2023**, midday, when a maximum temperature of 35 °C was recorded in Bucharest, Romania [46].

Figure 55. Visualising and recording the piezoelectric response on the scopemeter

The compressor, driven by a DC motor at 2500 rpm with ±20 rpm variation, operates in quasi-stationary mode. The frequency component of the male rotor, found at ~83 Hz, was extracted from the vibration spectra, and was chosen due to its stability and higher amplitudes [41], [42]. The resonant frequency of the piezoelectric transducer had to be pre-adjusted in laboratory (Figure 56), from ~210 Hz to 83 Hz, with an inertial mass of 7.3 g [47], in order to have a closer starting point for the adjusting required when taking the PEH on the compressor. The laboratory tests are prone to limitations compared to testing on the compressor.

a) 

b) 

Figure 56. Laboratory tests and voltage response displayed on spectrum analyser

A magnetic mount was used on the compressor. Point 1 was chosen as mounting spot for the tests with the piezoelectric harvesting system. A real-time frequency tuning of the PEH was necessary to match the compressor's frequency component as closely as possible, for maximum piezoelectric output. The mass elements were weighted at 9.0 g (Figure 57 left). A thermographic image in Figure 57 right marks a maximum of 65.2 °C on the compressor housing near the PEH mounting spot. The beam temperature of 49 °C is high for longer operation period [48].

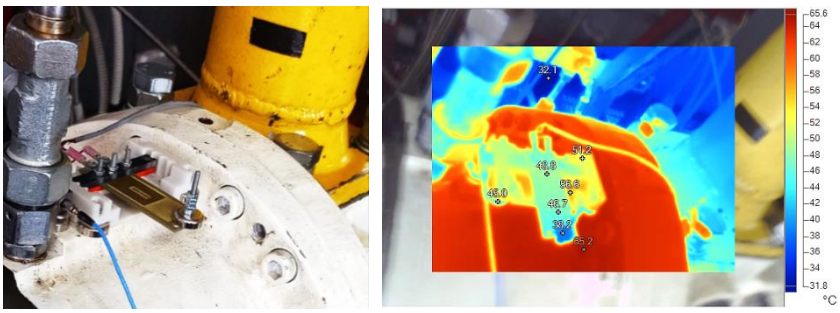

Figure 57. Piezoelectric harvester mounted on compressor (left) and thermographic image (right)

The piezoelectric voltage response was recorded (Figure 58 left). A zoom-in on the voltage range recorded in the left graph is presented in the right, providing an insight on the quasi-sinusoidal piezoelectric output.

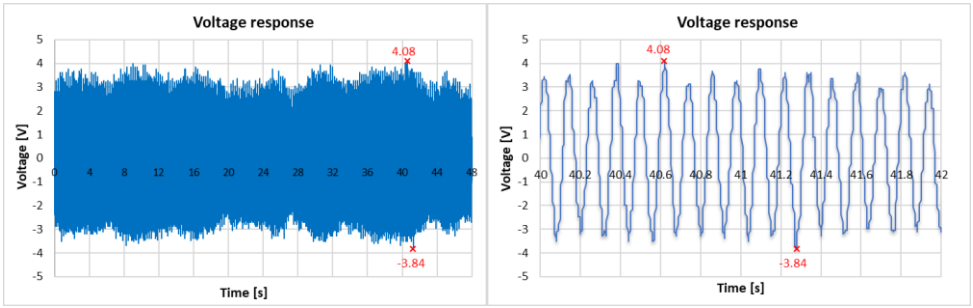

Figure 58. Piezoelectric quasi-sinusoidal voltage response recorded (left) and zoom in (right)

The maximum measured output parameters are summarized in Table 5 below

Table 5. Measured piezoelectric output parameters

Symbol	Quantity	Value	U.M.
V_{max}	Maximum AC voltage	4.08	V
I_{RMS}	Maximum RMS current	514.9	µA
P_{RMS}	Maximum RMS power	1.485	mW
f	Frequency	83 ± 1	Hz

7.2. Thermoelectric system harvesting the heat of a rotary screw compressor

Two TEGs were screw mounted, with heatsinks, onto the gearbox (). A replacement cover was physically executed. The tests were conducted on **6th June 2023**.

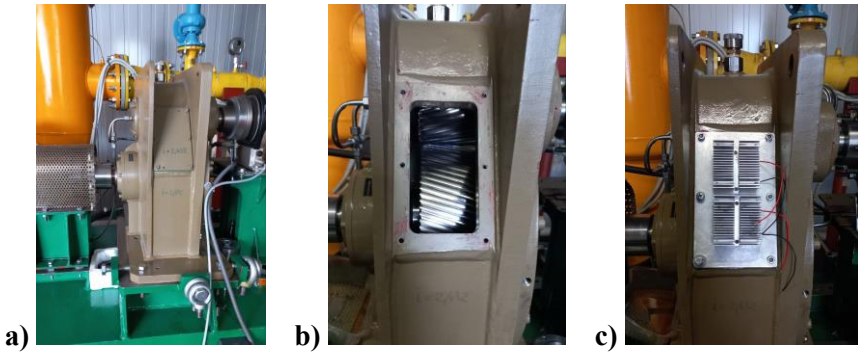

Figure 59. a) Gearbox with original cover, **b)** Gears inside, **c)** TEGs installed on duplicate cover

These steps for preparing TEGs are illustrated in the images below within Figure 60.

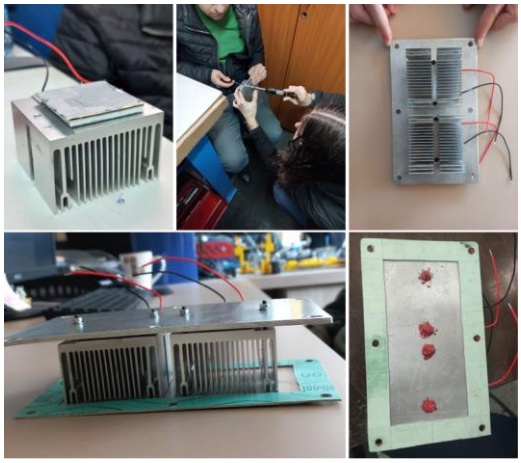

Figure 60. Work stages for preparing the thermoelectric harvesting system for installation

Thermographic images were taken to assess the operation conditions for the two thermoelectric modules. The lower module was labelled TEG1, and the upper module was labelled TEG2. The differences in the electric outputs are explained by Figure 61, that clearly outlines a higher temperature occurring in the upper half of the gearbox cover.

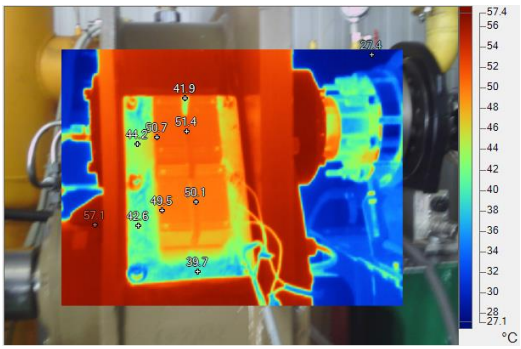

Figure 61. Thermographic scanning of the two TEGs on the gearbox cover

The thermographic image of TEG1 in Figure 62 left, taken transversally from below, reveals a temperature difference of ~2.1 °C across TEG1 module. A higher temperature gradient of ~5.6 °C across TEG2 module is observed in Figure 62 right, taken transversally from above.

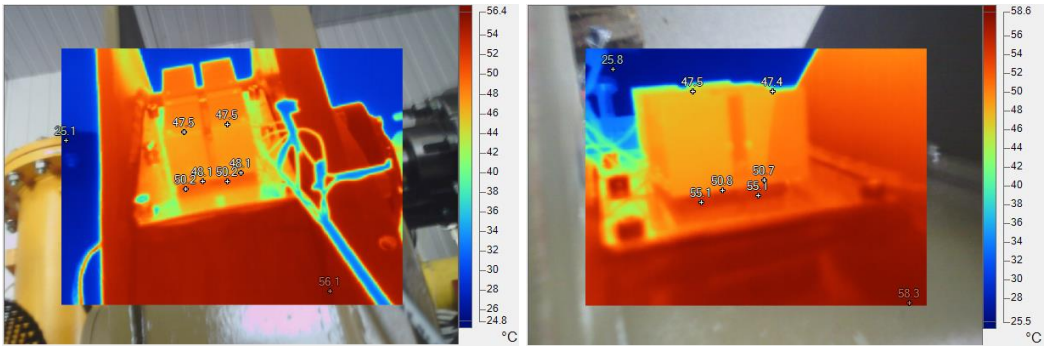

Figure 62. Thermal image of lower TEG1 (left) and upper TEG2 (right)

The graph in Figure 63 shows the separate voltage outputs rendered by the two thermoelectric modules. As expected from the thermal analysis, even though they start from about same voltage outputs, TEG2 reaches up to a higher maximum voltage produced than TEG1 after the thermal stabilization of the compressor.

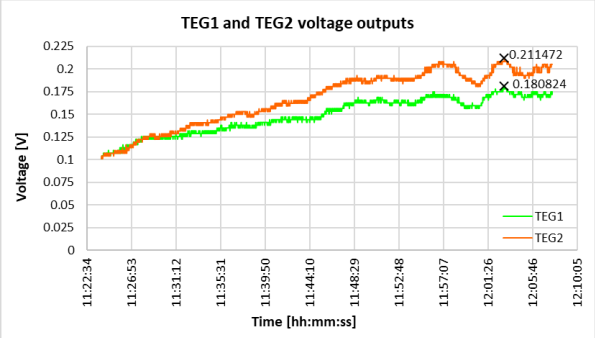

Figure 63. Separate voltage outputs from the two thermoelectric generators installed

The two modules were connected in series (Figure 64) showing the summed voltage output. The series connection was done after the separate measurement, when the compressor was already thermally stable. The series current was measured at 115 mA with the multimeter.

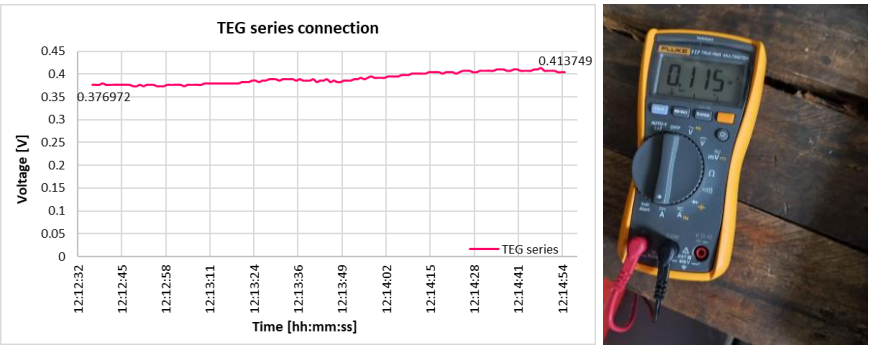

Figure 64. Voltage and output from the thermoelectric generators connected in series

The thermoelectric current is much higher than the piezoelectric current, of the order of hundred milliamperes compared to microamperes. The thermoelectric generators show a greater stability and easiness, also having the advantage of an output in direct current for powering low consumption devices. This gives thermoelectric generators a higher robustness, output consistency and standalone potential. Piezoelectric energy harvesters, on the other hand, render a higher voltage response, but this occurring only at resonance, with a feeble current. The challenges are, nevertheless, intriguing and satisfying to research and find solutions for. Piezoelectric harvesters are unpredictable and difficult to control, thus an abundant source for new research, development and academic publishing, to the delight of researchers in this niche.

8. CONCLUSIONS, ORIGINAL CONTRIBUTIONS AND FUTURE RESEARCH

The present thesis demonstrates piezoelectric and thermoelectric energy harvesting systems, whose purpose is to harness the vibrations and the thermal heating of an industrial rotary screw compressor operating in quasi-stationary mode. The thesis shows all the steps conducted for taking these micro energy harvesting systems all the way through modelling, calculating, simulating numerically, laboratory testing, towards the real challenge of validating in industrially relevant environment. The piezoelectric response obtained from the preliminary tests on the compressor is promising for further experimental works.

The thesis addressed realistic simulations on digital twin models, validated experimentally, for piezoelectric and thermoelectric applications of converting vibrations and waste heat from an industrial rotary screw compressor. While the 3D simulated models rely on physical devices, the boundary conditions further consider measured data from the compressor.

The purpose of this thesis was not to model an ideal vibration and heat source, like most works in the literature, in order to obtain high values for the electrical parameters, but to assess what could practically be expected from these two micro energy harvesters in real industrial conditions, taking into account the most important parameters that may lower the conversion to electric energy, may have a negative influence on the materials and devices, and may even damage the harvesters.

To the authors' knowledge, after a very thorough literature survey, no work has been found to report a successful implementation of multisource energy harvesting with this combination of harvesters, on industrial machinery, considering the harsh working conditions that could impact the piezoelectric and thermoelectric responses.

Original and novel contributions

The thesis presents only research conducted by its author, related to the proposed topic, with the help of the acknowledged persons. I deem important to mention that the topic was chosen out of passion and awakened interest during my Master of Science degree, due to an intriguing subject – *micro energy harvesting and piezoelectricity* – that currently seems to bring never-ending research opportunities, directions and findings.

As originality and novelty research presented in this thesis, I mention:

- The temperature dependence analysis of the piezoelectric harvester's response.
- The shape optimization of the piezoelectric cantilever towards triangular section, with two novel analyses that have not been done before in the literature, namely assessing the response per unit volume of active material, as well as bringing the five structures to the same von Mises stress, for a more relevant comparison.
- Experimental tests with both the PEH and TEH systems in an industrially relevant environment, on a rotary screw compressor, reaching a TRL 6.
- Numerical simulations with measured data on the compressor, considering the real temperature and triaxial vibrations for both piezoelectric and thermoelectric models.
- To the author's knowledge, no published work in the literature has so far reported piezoelectric energy harvesting being implemented on an industrial compressor. Hence, this thesis represents a first step for taking the technology validated in laboratory towards in-situ applications.

For further insight on the original contributions, please see my published articles, disseminating the research topics presented in this thesis.

I did not have an ongoing project at my institute to take material or data from, and all the presented material is new and researched during my doctoral stage. During doctoral stage, I have worked on two project proposals, out of which one was granted as component part of "Nucleu" project **PN 23.12.09**, contract **31N/2023**. The component sub-project proposal, titled

"Piezoelectric and Thermoelectric Energy Harvesting System from Vibration and Heat, Regarding Powering Wireless Sensors (PiTEH)" was elaborated and submitted by this thesis' author, drd. engr. Claudia Irina Săvescu (Borzea), and I am sub-project responsible. The project is currently ongoing within a bigger merged project, *"Fundamental research regarding energy harvesting from wind, waste and geothermal heat, as well as from wastes and biomass"*.

Future research directions and aims

The conducted work opens new avenues for research and development to a higher technology readiness level. A wireless sensors node is envisaged to be power supplied by the harnessed energy, after testing with a demo circuit board for energy harvesting. Since compressor vibrations occur on all three axes, a triaxial accelerometer should be employed within future experiments. For this purpose, a measuring device supporting ICP (Integrated Circuit Piezoelectric) input shall be used.

A rectifying circuit for the piezoelectric harvesters has been designed and developed. The circuit employs Schottky diodes with low voltage drop (0.3 V per diode). Another diode is placed in parallel with the bridge, for not interrupting the whole circuit if one of the piezoelectric transducers is malfunctioning. This circuit will be used when two or more piezoelectric harvesters shall be electrically connected, for avoiding cancelling each other's responses if vibrating in antiphase.

Future research will focus on optimizing the two technologies for use in industrial environments, along with connecting the necessary circuitry for WSNs. As well, attention will be paid to any influencing factors that might decrease the responses or jeopardize the energy harvesting devices. Mitigating the risks shall be of utmost importance.

Since an optimal load can boost the piezoelectric power output with more than one order of magnitude, future works will also be addressing the differences between the digital twin, testing in ideal laboratory conditions, and industrial conditions with circuitry components required for powering an energy harvesting circuit.

Improvements in thermoelectric harvesting will be sought by introducing ventilation, both in practical works as well as within the numerical simulations, considering external forced convection. As well, the time dependent study shall be extended with an auxiliary sweep of the hot side temperature. An utmost improvement that shall undoubtedly be the first thing to consider for piezoelectric harvesters will be ensuring a proper cooling and distancing from the compressor housing.

SELECTIVE BIBLIOGRAPHY

[1] L. Dhakar, 'Overview of Energy Harvesting Technologies', in *Triboelectric Devices for Power Generation and Self-Powered Sensing Applications*, L. Dhakar, Ed., in Springer Theses. , Singapore: Springer, 2017, pp. 9–37. doi: 10.1007/978-981-10-3815-0_2.

[2] R. Dauksevicius and D. Briand, 'Energy Harvesting', in *Material-Integrated Intelligent Systems - Technology and Applications*, John Wiley & Sons, Ltd, 2018, pp. 479–528. doi: 10.1002/9783527679249.ch21.

[3] M. Choi, K. M. Farinholt, S. Anton, J.-R. Lee, and G. Park, 'Multi-source energy harvesting for wireless SHM systems', in *Industrial and Commercial Applications of Smart Structures Technologies 2013*, SPIE, Mar. 2013, pp. 73–82. doi: 10.1117/12.2011883.

[4] Y. Li, Y. Liu, X. Liu, X. Wang, and Q. Li, 'An energy extraction enhanced interface circuit for piezoelectric and thermoelectric energy harvesting', *IEICE Electronics Express*, vol. 16, no. 6, pp. 20190066–20190066, 2019, doi: 10.1587/elex.16.20190066.

[5] Z. Hu, J. Qiu, X. Wang, Y. Gao, X. Liu, Q. Chang, Y. Long, and X. He, 'An integrated multi-source energy harvester based on vibration and magnetic field energy', *AIP Advances*, vol. 8, no. 5, p. 056623, Dec. 2017, doi: 10.1063/1.5006614.

[6] K. Fan, Q. Tan, H. Liu, Y. Zhu, W. Wang, and D. Zhang, 'Hybrid piezoelectric-electromagnetic energy harvester for scavenging energy from low-frequency excitations', *Smart Mater. Struct.*, vol. 27, no. 8, p. 085001, Jul. 2018, doi: 10.1088/1361-665X/aaae92.

[7] C. Borzea and D. Comeagă, 'Adjusting the Resonant Frequency of a Cantilever Piezoelectric Harvester', *Scientific Journal TURBO*, vol. V, no. 2, pp. 11–18, 2018.

[8] C. Borzea and D. Comeagă, 'Analysis and Optimization of a Piezoelectric Energy Harvester', *E3S Web Conf.*, vol. 112, p. 04001, 2019, doi: 10.1051/e3sconf/201911204001.

[9] C. Borzea, D. Comeagă, A. Stoicescu, and C. Nechifor, 'Piezoelectric Harvester Performance Analysis for Vibrations Harnessing', *UPB Scientific Bulletin, Series C: Electrical Engineering*, vol. 81, pp. 237–248, Aug. 2019.

[10] C. I. Borzea and C. D. Comeagă, 'Reliability of Euler-Bernoulli Model for Multilayer Composite Piezoelectric Beams', in *2019 11th International Symposium on Advanced Topics in Electrical Engineering (ATEE)*, Mar. 2019, pp. 1–6. doi: 10.1109/ATEE.2019.8724964.

[11] C. Săvescu, A. Morega, Y. Veli, and V. Petrescu, 'Numerical Modelling of Thermoelectric Energy Harvesting from Industrial Compressor Waste Heat', in *2023 13th International Symposium on Advanced Topics in Electrical Engineering (ATEE)*, Mar. 2023, pp. 1–6. doi: 10.1109/ATEE58038.2023.10108390.

[12] C. Savescu, V. Petrescu, D. Comeaga, R. Carlanescu, M. Roman, D. Lale, and A. Mitru, 'Thermal Potential of a Twin-Screw Compressor as Thermoelectric Energy Harvesting Source', *Engineering, Technology & Applied Science Research*, vol. 14, no. 2, Art. no. 2, Apr. 2024, doi: 10.48084/etasr.6417.

[13] D. Briand, E. Yeatman, and S. Roundy, 'Micro Energy Harvesting | Wiley', Wiley.com. [Online]. Available: https://www.wiley.com/en-us/Micro+Energy+Harvesting-p-9783527672929.

[14] P. Martín Sánchez, F. J. Rodríguez Sánchez, and E. Santiso Gómez, 'An Experimental Strategy for Characterizing Inductive Electromagnetic Energy Harvesters', *Sensors*, vol. 20, no. 3, Art. no. 3, Jan. 2020, doi: 10.3390/s20030647.

[15] Mc-Cast Engineering, 'Why is there water in my air compressor?' Accessed: Jan. 31, 2024. [Online]. Available: https://mc-castengineering.com/reports-blog-en/2019/11/27/why-is-there-water-in-my-air-compressor.

[16] CompAir, 'All About Oil Lubricated Air Compressor Technology'. Accessed: Jan. 31, 2024. [Online]. Available: https://www.compair.com/en-pk/technologies/oil-lubricated-air-compressor.

[17] P. Dineva, D. Gross, R. Müller, and T. Rangelov, 'Piezoelectric Materials', in *Dynamic Fracture of Piezoelectric Materials: Solution of Time-Harmonic Problems via BIEM*, P. Dineva, D. Gross, R. Müller, and T. Rangelov, Eds., in Solid Mechanics and Its Applications. , Cham: Springer International Publishing, 2014, pp. 7–32. doi: 10.1007/978-3-319-03961-9_2.

[18] C. R. Bowen, H. A. Kim, P. M. Weaver, and S. Dunn, 'Piezoelectric and ferroelectric materials and structures for energy harvesting applications', *Energy Environ. Sci.*, vol. 7, no. 1, pp. 25–44,

Dec. 2013, doi: 10.1039/C3EE42454E.

[19] APC, 'Piezoelectric Charge Constants'. Accessed: Feb. 16, 2024. [Online]. Available: https://www.americanpiezo.com/knowledge-center/piezo-theory/piezoelectric-constants.html.

[20] J. Ransley, 'Piezoelectric Materials: Understanding the Standards', COMSOL. Accessed: Feb. 19, 2024. [Online]. Available: https://www.comsol.com/blogs/piezoelectric-materials-understanding-standards/.

[21] COMSOL, 'Structural Mechanics Module User's Guide'. [Online]. Available: https://doc.comsol.com/6.1/doc/com.comsol.help.sme/StructuralMechanicsModuleUsersGuide.pdf.

[22] Midé Technology, 'PPA PRODUCTS Datasheet & User Manual'. [Online]. Available: https://cdn2.hubspot.net/hubfs/3841176/Data-Sheets/ppa-piezo-product-datasheet.pdf.

[23] R. Carter and R. Kensley, 'Introduction to Piezoelectric Transducers'. [Online]. Available: https://blog.piezo.com/hubfs/Manuals/Introduction-to-Piezoelectric-Transducers-Carter-Kensley.pdf.

[24] Virtual Amrita Laboratories, Amrita Vishwa Vidyapeetham University, 'Free Vibration of a Cantilever Beam (Continuous System) (Theory)'. Accessed: Feb. 16, 2024. [Online]. Available: https://vlab.amrita.edu/?sub=3&brch=175&sim=1080&cnt=1.

[25] M. A. Ahmad, A. M. Elshurafa, K. N. Salama, and H. N. Alshareef, 'Modeling of MEMS piezoelectric energy harvesters using electromagnetic and power system theories', *Smart Mater. Struct.*, vol. 20, no. 8, p. 085001, Jun. 2011, doi: 10.1088/0964-1726/20/8/085001.

[26] COMSOL, 'Time Dependent'. Accessed: May 07, 2024. [Online]. Available: https://doc.comsol.com/6.1/doc/com.comsol.help.comsol/comsol_ref_solver.35.016.html.

[27] National Instruments, 'Sound and Vibration Measurement Suite - NI', https://www.ni.com. Accessed: May 23, 2024. [Online]. Available: https://www.ni.com/docs.

[28] Piezo Systems, 'Material Properties - Thermal Dependency of Material Properties'. Accessed: Jun. 05, 2024. [Online]. Available: https://support.piezo.com/article/62-material-properties#thermal.

[29] C. Săvescu, D. Comeagă, and A. Stoicescu, 'Optimization of cantilever piezoelectric harvester to triangular shape with material reduction using finite element analysis', *Heliyon*, vol. 10, no. 13, p. e33209, Jul. 2024, doi: 10.1016/j.heliyon.2024.e33209.

[30] C. Borzea, D. Comeagă, Y. Veli, and A. Săvescu, 'Piezoelectric Cantilever Harvester with Trapezoidal/Triangular Section for Increased Conversion Efficiency', in *Iberian COMSOL Multiphysics Conference 2022*, Málaga, Spain, Jun. 2022, pp. 54–57.

[31] C. I. Borzea, C. D. Comeagă, and A. Săvescu, 'Boosting the Electric Output of a Cantilever Piezoelectric Harvester by Tip Curvature Blocking Elements', in *8th European Conference on Renewable Energy Systems (ECRES 2020)*, Istanbul, Turkey, Aug. 2020, pp. 344–350. [Online]. Available: https://www.ecres.net/proceedings_book_2020.pdf.

[32] Stanford Research Systems., 'Dynamic Signal Analyzer - SR785'. Accessed: Jun. 06, 2023. [Online]. Available: https://www.thinksrs.com/downloads/pdfs/catalog/SR785c.pdf.

[33] F. Membrini, 'A Brief History of Thermoelectrics | Mithras'. Accessed: Jul. 12, 2024. [Online]. Available: https://mithras.tech/2019/03/14/a-brief-history-of-thermoelectrics/.

[34] J. Dumitru, 'Contributions to the analysis and development of ambient energy harvesting systems (Orig. RO: Contribuții la analiza și dezvoltarea unor sisteme de recoltare a energiei ambientale)', Doctorate Thesis, Doctoral School of Electrical Engineering, University Politehnica of Bucharest, Bucharest, Romania, 2014.

[35] COMSOL, 'Thermoelectric generator', COMSOL. Accessed: Jul. 12, 2024. [Online]. Available: https://www.comsol.com/model/thermoelectric-generator-54111.

[36] M. Jaegle, 'Multiphysics Simulation of Thermoelectric Systems - Modeling of Peltier-Cooling and Thermoelectric Generation', presented at the COMSOL Conference 2008, Hannover, 2008. [Online]. Available: https://www.comsol.com/paper/multiphysics-modeling-and-development-of-thermoelectric-generator-for-waste-heat-61281.

[37] TEGpro, 'TE-MOD-10W4V-40 Datasheet rev. 1.0', Tegmart.com. [Online]. Available: https://www.tegmart.com/datasheets/TGPR-10W4V-40S.pdf.

[38] COMSOL, 'Thermoelectric Cooler Design App', COMSOL. Accessed: Jul. 16, 2024. [Online]. Available: https://www.comsol.com/model/thermoelectric-cooler-30611.

[39] 'COMSOL Multiphysics® Software - Understand, Predict, and Optimize', COMSOL. [Online]. Available: https://www.comsol.com/comsol-multiphysics.

[40] A. Prasad and R. C. Thiagarajan, 'Multiphysics Modeling and Development of Thermoelectric Generator for Waste Heat Recovery', presented at the COMSOL Conference 2018, Bangalore, India. [Online]. Available: https://www.comsol.com/paper/multiphysics-modeling-and-development-of-thermoelectric-generator-for-waste-heat-61281.

[41] C. Borzea, V. Petrescu, I. Vlăducă, M. Roman, and G. Badea, 'Potential of Twin-Screw Compressor as Vibration Source for Energy Harvesting Applications', *Electrical Machines, Materials and Drives - Present and Trends*, vol. 17, no. 1, Art. no. 1, 2021, doi: 10.36801/apme.2021.1.12.

[42] C. Săvescu, V. Petrescu, D. Comeagă, I. Vlăducă, C. Nechifor, and F. Niculescu, 'Vibration Analysis of a Twin-Screw Compressor as a Potential Source for Piezoelectric Energy Harvesting', *Revue Roumaine des Sciences Techniques - Série Électrotechnique et Énergétique*, vol. 68, no. 3, Art. no. 3, Oct. 2023, doi: 10.59277/RRST-EE.2023.3.1.

[43] G. M. Guttmann, Y. Gelbstein, G. M. Guttmann, and Y. Gelbstein, 'Mechanical Properties of Thermoelectric Materials for Practical Applications', in *Bringing Thermoelectricity into Reality*, IntechOpen, 2018. doi: 10.5772/intechopen.75476.

[44] 'Thermoelectric Cooler', COMSOL. [Online]. Available: https://www.comsol.com/model/thermoelectric-cooler-30611.

[45] 'COMSOL Multiphysics Reference Manual. Version: COMSOL 6.2.' [Online]. Available: https://doc.comsol.com/6.2/doc/com.comsol.help.comsol/COMSOL_ReferenceManual.pdf.

[46] AccuWeather, 'Bucharest, Romania Monthly Weather (July 2023)'. Accessed: Jul. 29, 2024. [Online]. Available: https://www.accuweather.com/en/ro/bucharest/287430/july-weather/287430

[47] C. Săvescu, D. Comeagă, A. Morega, and Y. Veli, 'Experimental Tests with Piezoelectric Harvester for Tuning Resonant Frequency to Vibrating Source', *Revue Roumaine des Sciences Techniques - Série Électrotechnique et Énergétique*, vol. 67, no. 4, Art. no. 4, Dec. 2022.

[48] C. Borzea, A. Morega, D. Comeagă, and Y. Veli, 'Temperature Influence on the Performances of a PZT-5H Piezoelectric Harvester', in *2021 12th International Symposium on Advanced Topics in Electrical Engineering (ATEE)*, Bucharest, Romania: IEEE, Mar. 2021, pp. 1–6. doi: 10.1109/ATEE52255.2021.9425102.